Accelerated Durability Characterization of Laminated Polycarbonate Systems

Samuel G. Riddle

Thesis submitted to the faculty of the Virginia Polytechnic Institute and State University in partial fulfillment of the requirements for the degree of

Master of Science
In
Engineering Mechanics

Scott W. Case, PhD, Chair
David A. Dillard, PhD
Michael J. Bortner, PhD

July 29, 2024
Blacksburg, VA

Accelerated Durability Characterization

of Laminated Polycarbonate Systems

Samuel Riddle

Abstract

Glass has long been used in glazing applications because of its transparency, stiffness, hardness, resistance to corrosion, and recyclability. Despite these useful features, however, glass is a very brittle material, lacking the ability to usefully absorb energy. Multi-material laminates have been produced as an alternative for glazing applications to improve energy absorption and other functionality requirements. As the demand for these laminates has increased in the construction, automotive, and defense sectors, a need for a more durable system has become apparent. One such example is the laminated glass systems often used in automobiles where two sheets are bonded (laminated) together with a plastic interlayer. Several types of interlayers have been used for these laminated systems, with polyvinyl butyral (PVB) being the most prevalent. A more recently developed interlayer type is thermoplastic polyurethane (TPU), which has the ability to bond to substrates other than glass, making it useful for applications like ballistic-resistant glass laminates, which often involve sheets made of polycarbonate. This study aims to explore the durability of laminated polycarbonate systems by investigating the interaction of environment and TPU viscoelastic behavior on the time-dependent crack growth in these laminates.

The main test utilized is the wedge test, a type of double cantilever beam (DCB) test in which a constant deflection is applied to characterize Mode I fracture behavior. The crack growth in wedge test specimens with different TPUs is evaluated at various temperature and humidity conditions over time. Dynamic mechanical analysis (DMA) is conducted to determine the thermomechanical properties of the TPUs. These properties are then used to analyze the results of the wedge tests. In addition to different TPU types, the effect of edge seals and surface treatment to improve bonding are compared.

Methods are explored for calculating the energy release rate, G (the rate at which the energy stored in a cracked body decreases as the surface area created by the crack increases) for a wedge specimen with a relatively thick, incompressible, and viscoelastic adhesive. The Irwin-Kies relationship is used to derive expressions for G.

Simple beam theory is first applied, assuming the two adherends of the wedge sample act as cantilever beams. Corrections are made on the simple beam theory expression to account for the effective opening displacement of a wedge specimen with a relatively thick adhesive, resulting in values of G that differ by nearly an order of magnitude. The compliance of the adhesive is then considered using Winkler's beam on elastic foundation model, which models the adhesive foundation as a system of independent springs. Because this method assumes a Poisson's ratio of zero, finite element analysis is employed to account for the nearly incompressible nature of the TPU. The resulting energy release rates using the beam on elastic foundation model show significant differences from those calculated using simple beam theory.

Accelerated Durability Characterization

of Laminated Polycarbonate Systems

Samuel Riddle

General Audience Abstract

Glass has long been used in glazing applications because of its transparency, stiffness, hardness, resistance to corrosion, and recyclability. Despite these useful features, however, glass is a very brittle material, lacking the ability to usefully absorb energy. Multi-material laminates have been produced as an alternative for glazing applications to improve energy absorption and other functionality requirements. As the demand for these laminates has increased in the construction, automotive, and defense sectors, a need for a more durable system has become apparent. One such example is the laminated glass systems often used in automobiles where two sheets are bonded (laminated) together with a plastic interlayer. Several types of interlayers have been used for these laminated systems, with polyvinyl butyral (PVB) being the most prevalent. A more recently developed interlayer type is thermoplastic polyurethane (TPU), which has the ability to bond to substrates other than glass, making it useful for applications like ballistic-resistant glass laminates, which often involve sheets made of polycarbonate. This study aims to explore the durability of laminated polycarbonate systems by investigating the interaction of environment and TPU viscoelastic behavior on the time-dependent crack growth in these laminates.

The main test utilized is the wedge test, where a wedge is inserted between two polycarbonate adherends bonded together with an interlayer. The wedge causes a debond (a crack) to form. This crack may then grow over time. The crack growth in wedge test specimens with different TPUs is evaluated at various temperature and humidity conditions. A separate test, referred to as dynamic mechanical analysis (DMA), is conducted to determine the thermomechanical properties of the TPUs. These properties are then used to analyze the results of the wedge tests. In addition to different TPU types, the effects of edge seals and surface treatment to improve bonding are compared. Models are used to analyze the resulting data to support the prediction of lifetimes of laminated polycarbonate systems employing the TPUs investigated.

Acknowledgements

I would like to thank the co-chairs of my committee, Dr. Scott Case and Dr. David Dillard, for their support during my time as a graduate student through its many twists and turns. Their patience and eagerness to help me along the way has been inspirational. I am also thankful to Dr. Michael Bortner for his willingness to participate on my committee.

This project would not have been possible without the funding of JNI Armor. I am thankful for the many conversations I have had via Zoom with David Jungk of JNI Armor and Chris Key and Joshua Gorfain of General Dynamics.

I would like to thank my colleagues in the Adhesion Mechanics Lab, including Christopher Jackson, Doug Hartley, and Dallas McKinney, for their help in conducting experiments. I am especially grateful to Zachary Teter for his assistance in conducting wedge test experiments.

My parents, Jeff and Llewellyn Riddle, receive the greatest thanks. They were my first teachers – in math, science, history, English, music, and more – and continue to be my greatest supporters and advisors. They also provided me with some of the best classmates a kid could have, whom I must also thank for their love and support, along with their spouses – James and Hannah Hodges, Brendon and Lydia Darby, Isaiah Riddle, and Joseph Riddle.

I am also thankful for the many friends who have supported and prayed for me along the way, especially those from the Reformed University Fellowship at Virginia Tech, Redeemer Associate Reformed Presbyterian Church of Blacksburg, VA, and Christ Reformed Baptist Church of Louisa, VA, as well as my colleagues at Grace Christian School in Staunton, VA.

This work is dedicated to my students at Grace, who reminded me that learning can be fun.

Table of Contents

List of Figures

1 Introduction

1.1 Motivation

Glass has long been used in glazing applications for its transparency, stiffness, hardness, resistance to corrosion, and recyclability. Despite these useful features, however, glass is a very brittle material, lacking the ability to usefully absorb significant energy or plastically deform. Multi-material laminates involving glass have been produced to improve energy absorption and other functionality requirements. As the demand for these laminates has increased in the construction, automotive, and defense sectors, a need for a more durable system has become apparent [1]. Laminated glass has appeared in the last century as a solution to this problem, with the first patent for laminated glass filed by Wood in 1905 with an application to car windshields [2]. Bonding at least two layers of glass to one another with an adhesive interlayer results in a glass laminate that is more capable of energy absorption and less prone to splintering when subjected to a localized kinetic energy. Additional layers strengthen the laminate but add weight that is undesirable for some applications [3].

Several types of interlayers have been used for laminated glass systems. Polyvinyl butyral (PVB) has historically been the most commonly used interlayer since it is relatively easy and inexpensive to manufacture [4]. Other interlayers include ionomers and ethylene-vinyl acetate (EVA) [1]. A more recently developed interlayer type is thermoplastic polyurethane (TPU). Perhaps the most significant difference between TPUs and PVBs is the ability of the TPU to bond to substrates other than glass. For this reason, TPUs are the most commonly used interlayers for applications like ballistic-resistant glass laminates, which include other transparent layers such as polycarbonate for its light weight and high resistance to shattering upon impact [1, 3].

When exposed to harsh environmental conditions, these bonded systems can be prone to delamination spurred by weathering agents including temperature and humidity. It is important, therefore, to study the durability of these systems when exposed to these conditions, even if those systems meet ballistic requirements [5]. Several studies have been conducted on the durability and resistance to aging of laminated ballistic-resistant glass systems with PVBs [1], but additional studies exploring these systems with TPUs are needed, as these systems are being more extensively utilized. This study will explore the durability of laminated TPU systems by employing a number of tests to investigate the interaction of TPU viscoelastic behavior and environment on the time-dependent crack growth in these laminates and evaluate the methods used to analyze these tests.

1.2 Previous studies on laminated glass durability

Methods to characterize the durability of laminated glass systems and their resistance to delamination have previously varied from study to study and have largely been based on trial and error. Grujicic notes that "the lack of basic understanding of the deformation/fracture behavior of transparent armor materials and the effect of their interactions/integration has resulted in the absence of basic design guidelines/principles for these complicated ballistic-protection systems" [6]. Merrill states that "delamination is only known as a snapshot … but there is little data about environments, rate of delamination, etc." [7] Several factors are believed to contribute to delamination in ballistic glass including temperature, humidity, chemical environment resulting

from exposure to potting materials, and the manufacturing process [7]. Within the past decade, various attempts have been made to categorize the different methods, often by focusing on one or more of these contributing factors to delamination.

Martín outlines some common techniques reported in the literature that have been used for glass laminate material characterization [1]. These techniques can be separated into two groups: studies on interlayers exclusively and studies on laminated systems. To study interlayers exclusively, some common methods are uniaxial tensile and compression tests to determine properties like Young's modulus, Poisson's ratio, and yield strength. Dynamic mechanical analysis (or DMA) is commonly used to characterize the viscoelastic behavior of the materials. For laminated systems that include materials other than the interlayer, Martín highlights methods including four-point bending tests and peel tests [1].

Many tests in the available literature focus on the durability of interlayers exclusively. Centelles [8] used a number of tests to characterize various material properties of PVB, EVA, and TPU interlayers under different aging conditions and strain rates. Three major techniques were explored. First, differential scanning calorimetry (or DSC) was used to determine the glass transition temperature of the interlayers. In this method, the heat flow in or out of a sample is measured over a temperature range. Polyurethanes are two-phase systems that typically exhibit two glass transition temperatures corresponding to a hard phase and a soft phase. The soft phase typically has glass transition temperatures below most service conditions, allowing the polymer to maintain flexibility and toughness. The hard phase dissociates at processing temperatures, allowing the material to flow, wet, and adhere to substrates. DSC was the sole focus of Frick and Rochman's work to characterize TPUs commonly used in ballistic glass systems [9]. Secondly, the water absorption of the interlayers was studied by immersing rectangular cut-outs of the interlayer films in water and measuring their weights over time. Thirdly, uniaxial tensile tests were used on water-immersed dogbone specimens. The studies consistently showed that toughness and strength of TPUs are less affected by aging than PVBs.

MacAloney proposed similar methods for testing and characterizing interlayer materials, including DSC and tensile testing on dogbone samples [10]. In addition to the moduli obtained through DMA, shear rheometry was used as a method to characterize the shear storage modulus and shear loss modulus of TPUs. Digital image correlation (DIC) methods were also used in tensile tests on dogbone samples and in compression tests on cylindrical samples. While providing some useful methods for characterization of interlayer films, laminated systems were not considered in these studies [8-10].

Several studies have been conducted beyond just the interlayer films and have explored the effects of temperature, moisture, and loading rate on laminated systems. The most common method in the literature for studying the durability of the adhesive joints in laminated glass systems appears to be a single lap joint test loaded in tension, where a testing rig is used to apply a shear force at different loading rates in order to obtain stress-strain curves and the shear moduli [11, 12]. The shear modulus is an important property to obtain according to Eliášová since "the composite action of laminated glass under loading is influenced mainly by the shear modulus of the interlayers." [13] This single lap shear test has been used to study a number of interlayers including PVBs, EVAs, and TPUs, and a number of systems with different adherends including two glass adherends [11, 13] and two polycarbonate adherends [12].

These single lap shear tests allowed the durability of laminated systems to be characterized when a mechanical stress was applied, but largely ignored the long-term delamination effects caused by temperature and humidity. Rivers and Cronin chose to eliminate external mechanical loads entirely and observe only the delamination caused by environmental factors (although mechanical loads caused by the environmental factors were still present) [14]. Relatively small samples of 2.4" (60 mm) length, 0.5" (12.75 mm) width and 0.2" (4.8 mm) thickness were made by bonding one layer of float glass to one layer of polycarbonate with an interlayer film. The samples were then aged and exposed to varying temperature and moisture cycles. The delamination was observed and compared for different environmental conditions and interlayer types. Their results confirmed that delamination is a function of both the temperature and the moisture. They also observed two different failure forms in cavitation and interfacial delamination.

The wedge test has been proposed as a method to simultaneously combine both the influence of external mechanical stress and environmental factors. Merrill used this method to calculate the energy release rate and stress intensity factor for laminated systems with an induced mechanical stress while simultaneously exposed to various temperatures and humidity conditions. This method was proposed to further explore the effect of potting material exposure on these systems [7].

While some standards and design specifications have been produced for ballistic glass systems[15, 16], the study of their durability remains an evolving field. The best and most efficient methods are still being determined. In this study, several methods are shown, building on the cited literature.

1.3 Wedge tests

Three basic modes of fracture are used to describe the loading of a cracked body, as shown in Fig. 1. They are referred to as Mode I, Mode II, and Mode III fracture, or as opening mode, sliding mode, and tearing mode, respectively [17]. A crack can result due to a single mode of fracture or any combination of the three.

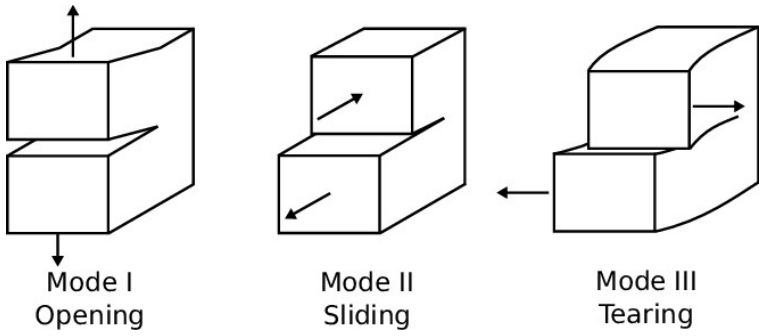

Fig. 1: The three fracture modes: Mode I (opening), Mode II (sliding), and Mode III (tearing). (Image from [18])

The wedge test is a type of double cantilever beam (DCB) test that has been a common method for analyzing Mode I fracture and adhesive properties of multi-layer systems since its initial use by Obreimoff in 1930 to study the splitting strength of mica [19, 20]. Searching for an inexpensive yet reliable and easily repeatable method to quantify the durability of surface-treated aluminum alloys used in aircraft when exposed to harsh environments, Boeing popularized the wedge test in the industrial field in the 1970s [21]. Consequently, the test is commonly referred to in the literature as the Boeing wedge test. Over the next several decades, the wedge test increased in use, especially to explore the bonding of aluminum alloys in aircraft applications [22-25], eventually leading to its standardization in ASTM D3762 (a standard which was subsequently withdrawn, but continues to be used) [26].

According to ASTM D3762, the wedge test specimens should consist of two adherends that are each 1.0" (25.4 mm) wide, 6.0" (152.4 mm) long, and 0.125" (3.2 mm) thick bonded together by an adhesive interlayer. On one end of the sample, 0.75" (19.1 mm) is left with no adhesive between the two adherends, creating an initial debond. An aluminum or stainless-steel wedge with the same thickness as the adherend is inserted on this end of the sample, essentially creating two cantilever beams subjected to a fixed displacement. When the adherends are separated from one another, the adhesive layer is subjected to a stress state that will result in cohesive, interfacial, or adherend failure [27]. The resulting crack length is observed over time as it advances through the specimen, and thereby the energy release rate (a property discussed in detail in the following sections) driving the fracture is calculated. Since the displacement caused by the wedge is fixed, the applied load as well as the energy release rate decreases as the crack grows. The proper method for the measurement of the crack length is debated, although various methods have been proposed, including the use of a microscope and simple observation by the naked eye. The challenge in precise measurement has resulted in some eliminating the need for an exact crack length measurement entirely by using a tapered wedge specimen [23, 28].

The wedge test has several advantages. It is relatively inexpensive and easy to create specimens and requires no sophisticated instrumentation. In addition, several specimens can be tested concurrently at varying exposure conditions, including temperature and humidity [29].

The mechanics of the wedge test were initially presented in 1986 by Cognard [30], who examined wedge specimens with stainless steel adherends bonded together by an epoxy resin called ASU 613. Cognard's specimens were relatively small, with adherends with a thickness of just 0.02" (0.5 mm), a width of 0.4" (10 mm), and a length of 1.6" (40 mm). Assuming that the wedge specimen is essentially a double cantilever beam subjected to a fixed displacement, Cognard applied simple beam theory (or Euler-Bernoulli beam theory) in order to calculate the energy release rate of his wedge test specimens. To apply simple beam theory to the wedge test, some assumptions must be made. The adherends are assumed to be cantilevered or fixed at the crack tip, thus neglecting root rotation and displacement. The adherends are further assumed to be linearly elastic and to not experience any sort of twisting, anticlastic bending, or plastic deformation [31, 32]. Arnott and Kindermann state that for many specimens, the plastic deformation of the adherends is one of the biggest issues with extracting meaningful results from the wedge test [28, 33]. The wedge itself is also assumed not to ride up against the adhesive.

While these assumptions are reasonable for specimens used by Cognard and others, they become more concerning with thicker or softer interlayers. Elastomeric adhesives, such as those used in laminated glass applications, result in a higher compliance for a wedge test specimen and

noticeable deflections near the root of the debond. Under fixed displacement loading conditions, a higher compliance will decrease the energy release rate below what would have been calculated by simple beam theory. In addition, the viscoelastic and therefore time and temperature dependence of an elastomeric adhesive will alter its mechanical properties at different testing conditions. These effects are particularly confounding because of the gradual growth in debond length, the oscillatory nature of the stress state ahead of the crack tip, and their combined effect. These concerns are addressed in the following sections.

1.4 Fracture mechanics

Two major mathematical methods have traditionally been used to evaluate the fracture of cracked members. The earliest of these was an energy approach taken by Griffith in the early twentieth century [34]. Griffith's approach defined a property called the energy release rate, *G*. It is defined as the rate at which the potential energy of a component is dissipated, or released, as the surface area of the crack increases [35]. Elsewhere, it is described as the driving force for delamination [36, 37]. The actual calculation of *G* can be quite complex, as it is dependent on several things including the component geometry, the material properties, and the load application. For a wedge test, it can be derived by analyzing the energy stored in a wedge specimen.

The total amount of potential energy, Π, is equal to the strain energy, *U*, creating the crack minus the external work (force, *P*, times displacement, Δ) applied to the body.

$$\Pi = U - P\Delta \tag{1}$$

Several studies have used Eq. (1) to derive the energy release rates of laminated systems with various geometries [30, 36-38]. For the case of the wedge test, where the displacement is held constant, then as the crack grows a distance *da*, the stiffness decreases (indicated by the subsequent curve with smaller slope), as shown in Fig. 2 for a linearly elastic system at a fixed displacement. A certain amount of energy (*dU*) is released from the member, and the total remaining energy is *U* – *dU*.

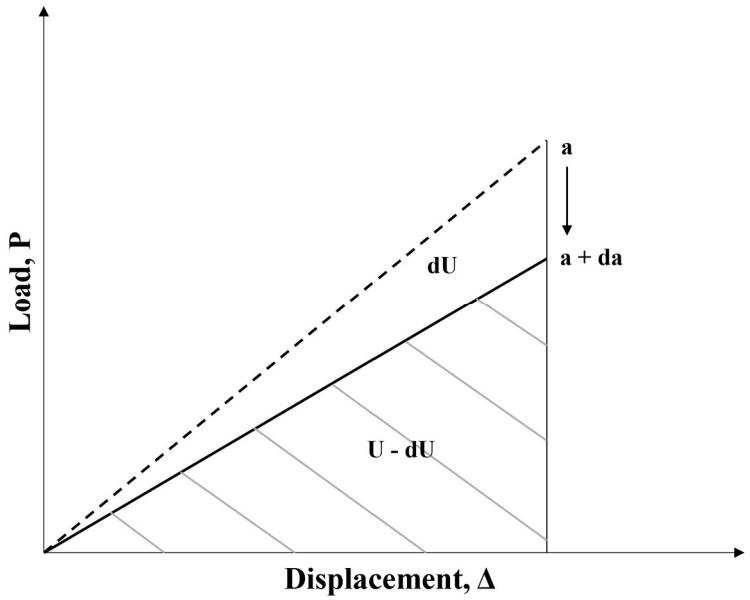

Fig. 2: Load versus displacement graph for a linear elastic system. The area under the curve is the stored energy in the material for the indicated displacement. (Image adapted from [35])

The rate at which the energy is decreasing as the surface area created by the crack increases is the energy release rate. The following definition can then be applied for a fixed displacement configuration [39].

$$G = -\frac{dU}{dA} \tag{2}$$

where G is the energy release rate, dU is the change in the strain energy, and dA is the increase in surface area created by the crack. It should be noted again that Eq. (2) is true only in the case of a fixed displacement with no external work.

The strain energy, U, is given by the area under the curve in Fig. 2 and can therefore be defined as

$$U = \frac{1}{2}P\Delta \tag{3}$$

for systems in which the load and deflection are linearly related. Substituting this definition for U into Eq. (2) (and remembering that the displacement, Δ remains constant) yields the following.

$$G = -\frac{1}{2}\Delta\frac{\partial P}{\partial A} \tag{4}$$

The compliance of a material, C, can be used to further expand this expression. Compliance is a measure of a material's readiness to deform and is essentially the inverse of the stiffness of the material. For a linear elastic system, the applied load is linearly proportional to the resulting displacement by a factor of the reciprocal of the compliance (known as the stiffness) [40]. The following definition can therefore be made.

$$P = \frac{\Delta}{C} \tag{5}$$

Substituting this expression into Eq. (4), in which P is differentiated with respect to the crack surface area produces the following.

$$G = -\frac{1}{2}\Delta\left(-\frac{\Delta}{C^2}\frac{\partial C}{\partial A}\right) \tag{6}$$

$$G = \frac{1}{2}\frac{\Delta^2}{C^2}\frac{\partial C}{\partial A} \tag{7}$$

A final substitution produces what is known as the Irwin-Kies equation for linear elastic systems [40, 41], which defines the energy release rate for a crack member in terms of the applied force, the compliance, the crack length, and the specimen's width.

$$G = \frac{1}{2}P^2\frac{\partial C}{\partial A} = \frac{1}{2}P^2\frac{1}{w}\frac{\partial C}{\partial a} \tag{8}$$

This important equation is utilized in the later sections to derive values for the energy release rate for wedge test specimens, including complications associated with adhesive thickness and compliance.

It should be noted that deriving the energy release rate from a case of constant load will also yield Eq. (8). In this case, G is defined in terms of the complementary strain energy, U^*.

$$G = \frac{dU^*}{da} \tag{9}$$

The complementary strain rate is defined as

$$U^* = -\frac{P\Delta}{2} \tag{10}$$

Plugging this expression into Eq. (9), this time assuming a constant P and variable Δ, will once again result in the Irwin-Kies equation. In fact, the Irwin-Kies equation is applicable for any linear elastic system, regardless of the nature of input load or displacement.

The second major mathematical method to evaluate the fracture of cracked members was introduced by Irwin in the 1950s [42]. Irwin introduced a property called the stress intensity factor, K, which is a mathematical tool that relates the stress near the crack tip to the component geometry of a linear elastic material. K is especially useful in predicting the failure of a material by calculating a critical stress intensity factor, K_c, which is also referred to as the fracture toughness.

Both G and K are used in engineering applications and are related as follows for cases of Mode I fracture in a linear elastic system [35].

$$G = \frac{K^2}{E_I} \tag{11}$$

where E_I is simply equal to E for plane stress and is defined below for plane strain using the elastic modulus, E, and Poisson's ratio, ν.

$$E_I = \frac{E}{1-\nu^2} \tag{12}$$

For the case of the wedge test, determining K from G is not as straightforward, since the wedge specimens involve the interfacial debonding of dissimilar viscoelastic (and therefore time and temperature dependent) materials. In this work, focus is given to the energy approach, which tends to be more commonly used for bonded systems.

1.5 Dynamic mechanical analysis

Polymers are viscoelastic, meaning that their mechanical behavior can be characterized as both viscous (like a liquid) and elastic (like a solid) [43-45]. To characterize a polymeric material, the degree to which it behaves like a liquid or a solid must be determined. Both the temperature and the timescale of an applied load play a role in the viscoelastic properties of a material [44]. Higher temperatures and longer timescales typically result in a more liquidlike behavior, whereas lower temperatures and shorter timescales result in more solid-like behavior. Properties like the stiffness of the material are therefore both time and temperature dependent.

A common method for characterizing the viscoelastic properties of a polymer is dynamic mechanical analysis or DMA [43]. In this method, an oscillatory force is applied to a small sample. As each oscillation is applied, the complex modulus of the polymer can be determined from the strain induced by it. In a frequency sweep, the temperature is held constant while the frequency of the oscillation varies. In a temperature sweep, the frequency is held constant while the temperature changes with each oscillation. Performing DMA on a polymer results in differing values of moduli over a range of temperatures or frequencies.

It should be noted that rather than determining the Young's modulus of a material, dynamic mechanical analysis gives a property called the dynamic (or complex) modulus, which is defined as follows.

$$E^* = E' + iE'' \tag{13}$$

where E' is the storage modulus, a measure of how elastic a material is or how easily it can store energy, and E'' is the loss modulus, a measure of the material's ability to dissipate energy. For a material in which the loss modulus is small compared to the storage modulus, the magnitude of E^* at the appropriate temperature and rate can be used as a good approximation for the Young's modulus [43]. As will be noted using dynamic mechanical analysis, this is the case for a TPU, and therefore the Young's modulus will be assumed in this thesis to be equal to the magnitude of the complex modulus during analysis. The ratio of the loss modulus to the storage modulus is referred to as $\tan\delta$, as shown below.

$$tan\ \delta = \frac{E''}{E'} \tag{14}$$

Because of the limited frequency ranges in dynamic mechanical analysis, a method called time-temperature superposition is often used to shift multiple frequency sweeps taken at different temperatures to create a final master curve with a larger range of frequencies. The WLF equation put forward by Williams, Landel, and Ferry in [46] is a popular method used to mathematically represent the temperature shift factors used in the development of the master curve. (For polyurethanes, it can be applied for temperatures at and above the soft phase glass transition temperature.) The WLF equation is defined as follows.

$$\log(a_T) = -\frac{C_1(T - T_{ref})}{C_2 + (T - T_{ref})} \tag{15}$$

where a_T is the thermal shift factor, T_{ref} is some reference temperature, and C_1 and C_2 are material constants that also depend on the reference temperature chosen. Creating a master curve of overlapping data over a range of frequencies is accomplished by manually shifting the frequency sweeps about this reference temperature, as described in [47]. This method was used in this study, and all DMA data is provided with a shift factor plot produced from the manual shifting, and the reference temperature is noted.

2 Experimental Set-up

2.1 Overview

Two primary test types were used to explore the durability of laminated polycarbonate systems. First and primarily, wedge tests were used to explore the fracture mechanics of the systems. Secondly, dynamic mechanical analysis (DMA) was used to explore the viscoelastic properties of the interlayers in these systems. The following sections detail the experimental methods and procedures for each of these tests.

2.2 Wedge tests

2.2.1 Overview

The samples for the wedge tests were provided by JNI Armor. Unless otherwise indicated, each sample consisted of two non-surface-treated polycarbonate adherends with thicknesses of 0.5” (12.7 mm) and an interlayer with a thickness of 0.075” (2.0 mm). Each sample had a width of 1.0” (25.4 mm) and a length of either 16.0” (406 mm) or 12.0” (305 mm). To make it easier to insert the wedge, one end of each sample had an unbonded region with a length of 1.0” (25.4 mm. Fig. 3 gives a schematic of the wedge test samples used for this study.

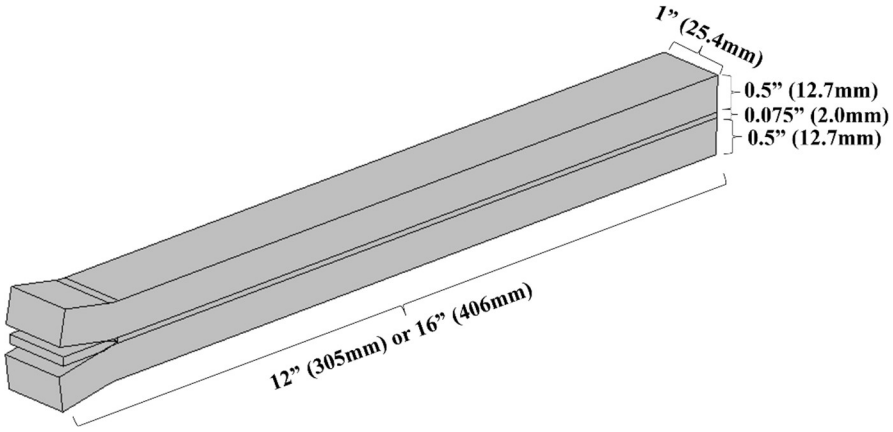

Fig. 3 Dimensions for wedge test sample. The length of the samples was 16" (406 mm) for dry samples and 12" (305 mm) for wet samples in order to accommodate them in the water baths.

Four different commercially available TPU interlayers and one EVA interlayer were studied. A summary of the interlayers with the approximate values of their secant moduli at 100% elongation at room temperature, determined by their respective manufacturers, is given in Table 1. Data sheets for the adhesives indicate the use of ASTM D412, which advises a strain rate of 0.1 min^{-1} for dynamic mechanical analysis [48]. TPUs 1 through 3 are designated as standard TPUs since they have similar secant moduli at 100% elongation at room temperature, based upon information provided by their manufacturers. The fourth TPU is referred to as a "stiff" TPU because its secant modulus at 100% elongation is nearly four times larger than the corresponding moduli for the other three TPUs. The stiffnesses and viscoelastic properties of each interlayer were further explored using dynamic mechanical analysis.

Table 1: A list of the interlayers used in the wedge tests with their secant moduli at 100% elongation at room temperature as provided by their manufacturers.

Interlayer type	Secant Modulus @ 100% Elongation @ 25°C (psi)	Secant Modulus @ 100% Elongation @ 25°C (MPa)
TPU #1	500	3.5
TPU #2	530	3.7
TPU #3	480	3.3
TPU #4	1700	11.7
EVA	2100	14.5

A stainless-steel wedge with thickness of 0.125" (3.2 mm) or dowel pin of diameter 0.125" (3.2 mm) was used to create the initial displacement between the adherends. The geometries of the wedges and dowel pins is shown in Fig. 4. The dowel pins were inserted into the samples as shown in Fig. 5.

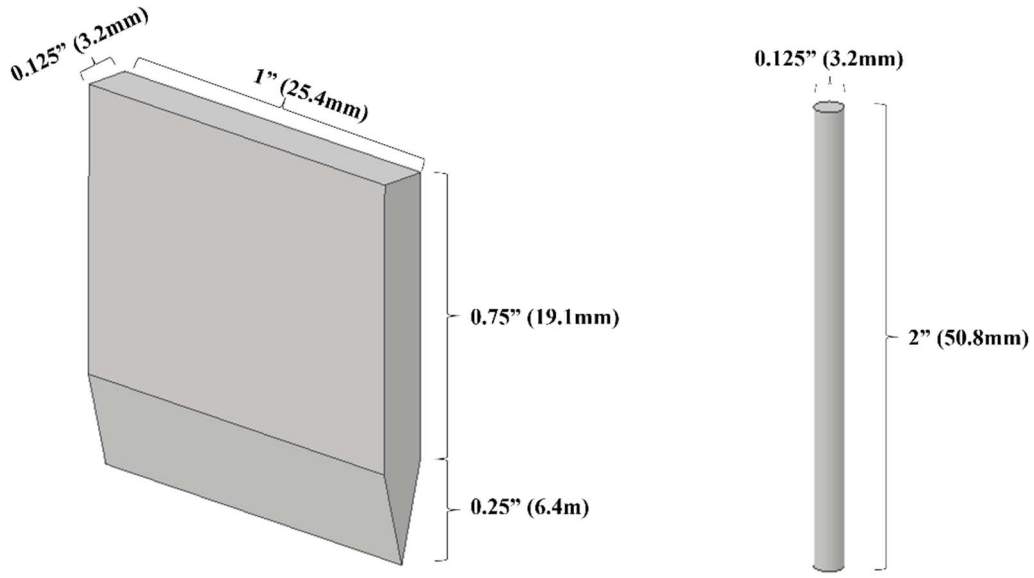

Fig. 4: Schematics of stainless-steel wedge (left) and dowel pin (right) used for wedge tests.

Fig. 5: Insertion of dowel pin into wedge test samples

After the wedge insertion, the samples were placed in several different temperature and humidity environments. Tests were conducted at 50°C, 65°C, and 75°C. Some samples were designated as dry samples and placed in an oven with ambient air heat to the specified temperatures with no humidity control. Others were designated as wet samples and suspended above the water in temperature-controlled water baths, as seen in Fig. 6.

Fig. 6: Dry wedge test samples held in oven at ambient laboratory conditions (left); Wet wedge test samples held suspended in water bath (right)

A complete summary of all the tests is given in Table 2 at the end of this section, noting the interlayer type, the temperature and humidity conditions, and the number of sample replicates for each test.

Crack length measurements were, in general, taken five times on the day of wedge insertion and afterwards taken once per day or every other day. Each time a measurement was taken, the crack growth was observed through the transparent adherend by the naked eye and marked directly on the adherend with a permanent marker. The furthest extent of debonding was marked with masking tape to take the measurement more easily, and the distance from the wedge tip or dowel pin to the tape was then measured using a pair of calipers, as seen in Fig. 7.

Fig. 7: Measurement of crack length from wedge tip to farthest extent of cavitation/debonding

2.2.2 Potting materials and edge seals

Moisture diffusion into a laminated glass system from its edges can lead to increased delamination. Just as an increase in temperature can create residual stresses due to the differing rate of expansion in a thermally mismatched system, moisture ingress can lead to the layers of a laminate expanding at different rates, causing delamination. In addition, moisture absorption could accelerate the aging of the materials and lead to plasticization [14]. Potting materials and edge seals have both been used to encapsulate laminated systems to hold the layers in place and to prevent moisture ingression. Potting material is defined in [49] as an encapsulating resin that involves a one-part or two-part system that typically requires a curing process. In addition to preventing moisture diffusion, potting material also helps to protect the laminate from high temperatures and provides cushioning from vibration. Edge seals, on the other hand, are a material used as a barrier to delay moisture ingress or slow diffusion and as an extra help to the adhesive in holding the system together [50]. For example, a metal edge seal would force moisture to move along a longer diffusion path. Both potting materials and edge seals have been used to delay moisture ingression leading to delamination in ballistic glass systems. While doing so, however, they could also be adding additional stresses to the system [51].

Three different potting materials were applied to the sides of some samples. In addition, some samples were provided by JNI Armor with three different edge seals applied along the lengths of the samples, as seen in Fig. 8.

Fig. 8: Wedge samples provided by JNI Armor with edge seals already applied.

2.2.3 Surface treatment

Various methods including mechanical abrasion or sand or grit blasting have been used to treat the surface of a material to enhance its adhesion [52]. An increasingly common method is the use of a plasma surface treatment. Plasma is an energized ionized gas that contains ions and free electrons that have the capability of gaining energy when exposed to an electric field [53]. When a solid material is exposed to a plasma, there can be a significant effect on its surface caused by the excited state of its ions and free electrons which can cause a reduction in the length of its molecules and the amount of cross-linking; however, the benefit is that molecular bonds on the surface are altered to include polar and other moieties to enhance the adhesion [52]. Li showed that cold plasma treatment has a positive effect on the performance of laminated glass using polyurethane, especially with samples undergoing an aging process [54]. A select number of wedge tests were conducted on specimens with plasma surface-treated adherends.

Table 2: Summary of wedge tests.

Interlayer	Temp.	Humidity	Potting Material	Edge Seal	# Replicates
TPU #1	50°C	Dry	None	None	3
TPU #1	65°C	Dry	None	None	3
TPU #1	75°C	Dry	None	None	3
TPU #1	50°C	Wet	None	None	3
TPU #1	65°C	Wet	None	None	3
TPU #1	75°C	Wet	None	None	3
TPU #2	50°C	Dry	None	None	3
TPU #2	65°C	Dry	None	None	3
TPU #2	75°C	Dry	None	None	3
TPU #2	50°C	Wet	None	None	3
TPU #2	65°C	Wet	None	None	3
TPU #2	75°C	Wet	None	None	3
TPU #3	50°C	Dry	None	None	3
TPU #3	65°C	Dry	None	None	3
TPU #3	75°C	Dry	None	None	3
TPU #3	50°C	Wet	None	None	3
TPU #3	65°C	Wet	None	None	3
TPU #3	75°C	Wet	None	None	3
TPU #4	50°C	Dry	None	None	3
TPU #4	65°C	Dry	None	None	3
TPU #4	75°C	Dry	None	None	3
TPU #4	50°C	Wet	None	None	3
TPU #4	65°C	Wet	None	None	3
TPU #4	75°C	Wet	None	None	3
EVA	50°C	Dry	None	None	3
EVA	65°C	Dry	None	None	3
EVA	75°C	Dry	None	None	3
EVA	65°C	Wet	None	None	3
EVA	75°C	Wet	None	None	3
TPU #1	50°C	Dry	Potting Material #1	None	3
TPU #1	65°C	Dry	Potting Material #1	None	3
TPU #1	75°C	Dry	Potting Material #1	None	3
TPU #1	50°C	Wet	Potting Material #1	None	3
TPU #1	65°C	Wet	Potting Material #1	None	3
TPU #1	75°C	Wet	Potting Material #1	None	3
TPU #2	65°C	Dry	Potting Material #1	None	3
TPU #2	75°C	Dry	Potting Material #1	None	3
TPU #2	50°C	Wet	Potting Material #1	None	3
TPU #2	65°C	Wet	Potting Material #1	None	3

TPU #2	75°C	Wet	Potting Material #1	None	3
TPU #1	50°C	Dry	Potting Material #2	None	2
TPU #1	65°C	Dry	Potting Material #2	None	3
TPU #1	75°C	Dry	Potting Material #2	None	3
TPU #1	50°C	Wet	Potting Material #2	None	3
TPU #1	65°C	Wet	Potting Material #2	None	3
TPU #1	75°C	Wet	Potting Material #2	None	3
TPU #2	50°C	Dry	Potting Material #2	None	2
TPU #2	65°C	Dry	Potting Material #2	None	3
TPU #2	75°C	Dry	Potting Material #2	None	3
TPU #3	50°C	Dry	None	Edge Seal #1	3
TPU #3	50°C	Dry	None	Edge Seal #2	3
TPU #3	50°C	Dry	None	Edge Seal #3	3
TPU #3	75°C	Dry	None	Edge Seal #1	3
TPU #3	75°C	Dry	None	Edge Seal #2	3
TPU #3	75°C	Dry	None	Edge Seal #3	3

2.3 Dynamic mechanical analysis

Dynamic mechanical analysis (DMA) was used to explore the viscoelastic properties of the various TPU films as well as two PVB films for comparison. Tests were conducted using tensile clamps in a TA Q800 DMA machine, as seen in Fig. 9. The tests consisted of temperature steps from -60°C to 75°C, with intervals of 5°C, and frequency sweeps from 1 Hz to 100 Hz at each temperature. Strain amplitudes ranged from 0.15% to 0.25%, within the linear viscoelastic range for a TPU [43]. After collecting frequency sweeps at each indicated temperature, shifting was performed manually. The reference temperature and shift factor plot are given for all the obtained DMA data.

Fig. 9: TA-Q800 DMA machine used for DMA testing to characterize viscoelastic properties of TPU films.

3 Results & Analysis

3.1 Wedge tests

3.1.1 Overview

As mentioned in section 1.4, delamination growth is often evaluated using the energy release rate, G, which is the driving force for delamination [36, 37]. For fixed displacement loading conditions, G is defined as the rate at which the stored elastic energy of a component is dissipated, or released, as the surface area of the sample caused by the crack increases. The Irwin-Kies equation can be used to calculate the strain energy release rate.

$$G = \frac{1}{2}P^2\frac{\partial C}{\partial A} = \frac{1}{2}P^2\frac{1}{w}\frac{\partial C}{\partial a} \tag{16}$$

The geometry of a general wedge sample is shown in Fig. 10, with dimensions labeled including the width (w) and thickness (e) of the sample, the thickness of the adhesive layer (h_a), the thickness of the wedge (h), and the sample length length (l).

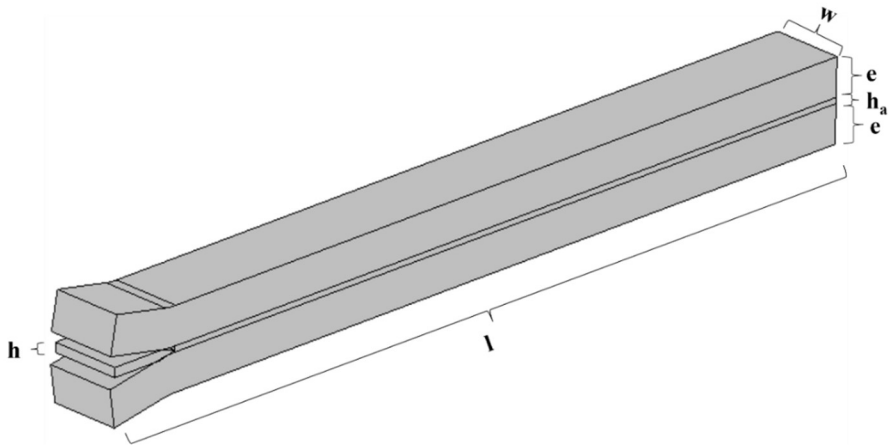

Fig. 10: Geometry of wedge test samples with dimensions labeled as seen in energy release rate calculations

It should be noted that h represents the entire thickness of the wedge and h_a represents the entire thickness of the adhesive. The midplane of the wedge sample is an assumed plane of symmetry which can be divided into two separate beams, each with an adhesive foundation that is half the thickness of the adhesive layer.

The following sections report the results and analysis obtained from the wedge tests with the experimental set-up described in section 2.2. The methods for analysis are first discussed by reviewing the derivations for G using two major methods: simple beam theory (SBT) and beam on elastic foundation (BoEF). The experimental data is then provided and analyzed using these methods.

3.1.1.1 Simple beam theory

As discussed in section 1.3, Cognard [30] used simple beam theory to calculate the energy release rate of a wedge specimen. He assumed the adherends of the wedge samples to be two symmetrical cantilever beams that were fixed at the crack tip. He also assumed the absence of twisting, anticlastic bending, and plastic deformation for the adherends and that the wedge itself did not to ride up against the adhesive. It is important to recognize that Cognard was analyzing metal adherends bonded by stiff epoxy resins with thicknesses of 20 μm or less [29, 30], significantly smaller than the adhesive layer in this study (2.0 mm). Additionally, epoxy typically has a stiffness that is several orders of magnitude greater than the TPU adhesives used in this work. The adhesive layer is therefore assumed to offer negligible thickness and compliance in Cognard's analysis. The necessary addition of the adhesive layer for a wedge sample with a TPU adhesive is discussed in the following section.

The geometry resulting from Cognard's assumptions, with the wedge specimen simplified as two cantilever beams, each with a fixed end at the crack tip, is seen in Fig. 11.

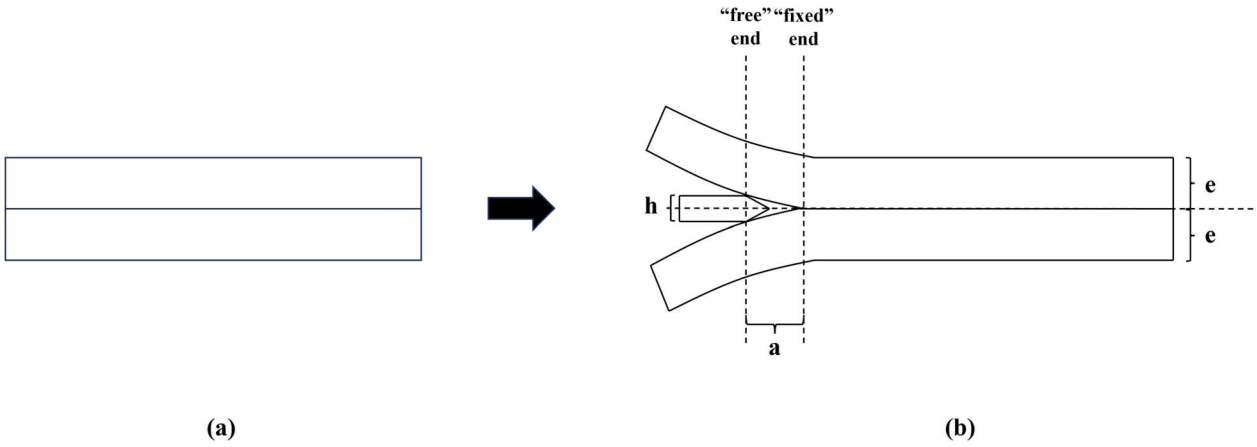

Fig. 11: Geometry of wedge test sample as cantilever beam for simple beam theory before (a) and after (b) wedge insertion. h *is the wedge thickness,* e *if the thickness of a single beam, and* a *is the crack length.*

To calculate the energy release rate, the geometry of Fig. 11 can be simplified as a single cantilever beam, as shown below.

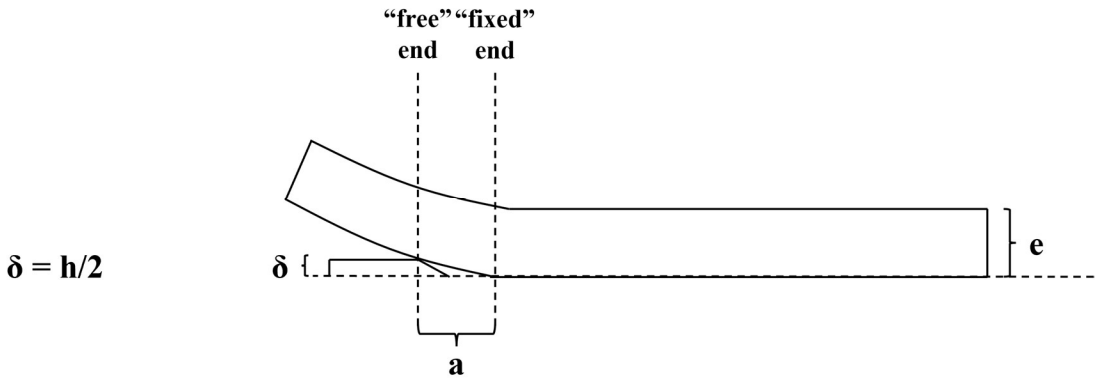

Fig. 12: Geometry of half of wedge test sample for simple beam theory. The deflection (δ) is defined as half the wedge thickness.

The total compliance of the specimen can then be determined as follows.

$$C = \frac{h}{P} = \frac{2\delta}{P} \tag{17}$$

According to simple beam theory, deflection for a cantilever beam with an applied force P on the free end of the beam is defined as:

$$\delta = \frac{Pa^3}{3EI} \tag{18}$$

where δ is the deflection of the beam, P is the applied load, a is the length of the beam (or the crack length in the case of the wedge test), E is the Young's modulus of the beam, and I is the second moment of area [55] of the cross section. The crack tip is again considered to be at the fixed end of the beam.

Differentiating C with respect to the crack length a yields the following.

$$\frac{\partial C}{\partial a} = \frac{\partial}{\partial a}\left(\frac{2}{P}\frac{Pa^3}{3EI}\right) = \frac{2a^2}{EI} \tag{19}$$

Substituting this into the Irwin-Kies equation produces the following expression for the energy release rate.

$$G = \frac{1}{2}P^2\frac{1}{w}\frac{2a^2}{EI} \tag{20}$$

A more useful expression for the energy release rate will be in terms of the deflection at the free end, since this deflection is a fixed quantity for the wedge test. Solving for P from Eq. (18) and substituting into Eq. (20) results in the following expression for G.

$$G = \frac{9EI\delta^2}{wa^4} \tag{21}$$

Further simplification can be made by substituting for the beam's second moment of area, defined as follows for a rectangular beam [35]:

$$I = \frac{we^3}{12} \tag{22}$$

where w is the width of the beam and e is its thickness. Substituting for this expression yields the following.

$$G = \frac{3}{4}\frac{Ee^3\delta^2}{a^4} \tag{23}$$

The expression $\delta = h/2$ can be substituted into this equation to account for the two symmetric beams that make up the wedge specimen. The final simplified definition, therefore, of the strain energy release rate of a full wedge specimen using simple beam theory where the adhesive thickness is assumed to be negligible is

$$G = \frac{3}{16}\frac{Ee^3h^2}{a^4} \tag{24}$$

where E is the elastic modulus of the adherend, e is the thickness of the adherends, h is the wedge thickness, and a is the crack length.

3.1.1.2 Effective opening displacement

Eq. (24) is the expression used by Cognard for metal adherends bonded by an epoxy resin with a thickness under 20 μm. It assumes that the adhesive layer between the two adherends is negligible and does not assume any effective spacing between the adherends. In the case of a thicker interlayer (such as the wedge geometry of this study, where the adhesive thickness is 2.0 mm), an effective opening displacement must be used, as shown in Fig. 13.

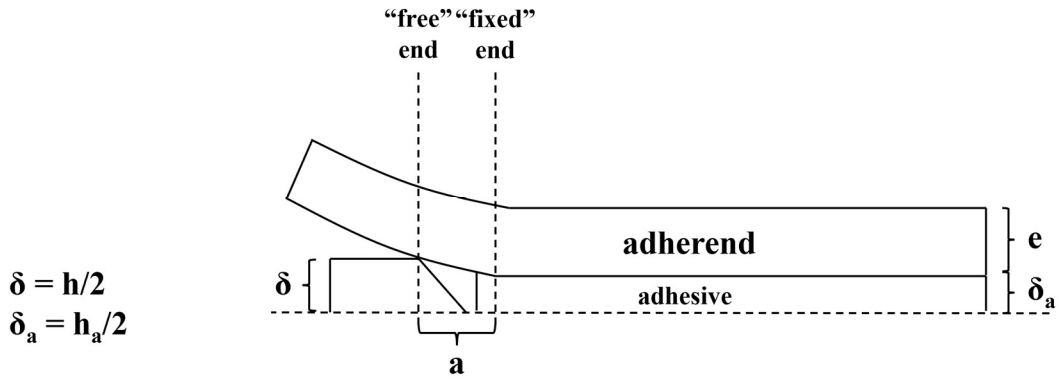

Fig. 13: Geometry of half of wedge test sample for simple beam theory with non-negligible adhesive layer. The deflection (δ) is defined as half the wedge thickness. The effective opening displacement (δ_a) is defined as half the adhesive thickness.

A simple correction can be made to Eq. (24) to account for the adhesive layer. The resulting equation is given below.

$$G = \frac{3}{16}\frac{Ee^3(h-h_a)^2}{a^4} \tag{25}$$

where h_a is the thickness of the adhesive. It should be noted that the assumptions for simple beam theory still hold for this equation. Merrill's analysis in [7] ignores the adhesive thickness of the wedge test despite its similarity to the geometry in this study, however, Fig. 14 shows the importance of its inclusion. The energy release rates of the wedge geometries used in this study are compared with the adhesive thickness included and ignored.

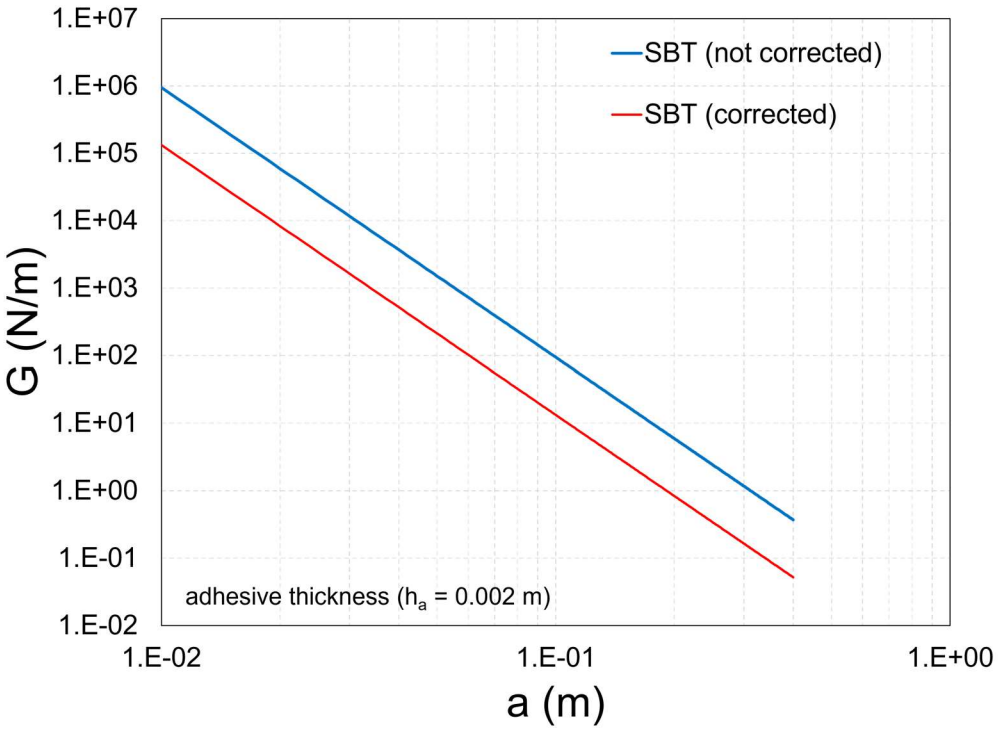

Fig. 14: Comparison of energy release rates for simple beam theory with and without correction for the adhesive thickness. When considering the geometry of the adhesive for the wedge test geometry of this study, the energy release rate decreases significantly.

The top curve in the figure represents the energy release rate calculated from Eq. (24), which ignores the adhesive thickness. The bottom curve is calculated from Eq. (25) and accounts for the adhesive thickness used in the wedge test (0.075" or 2.0 mm). Correcting for the adhesive in the case of the wedge tests used in this work causes a decrease of approximately 86% in the energy release rate (nearly an order of magnitude), indicating the importance of including this correction when considering a wedge test specimen with a thicker adhesive.

3.1.1.3 Beam on elastic foundation

While Eq. (25) accounts for the adhesive thickness, it does not consider the possible deflections that a compliant adhesive might cause at the crack tip. A more accurate model to calculate the energy release rate would account for the compliance of the foundation on which the beam sits. Such a model is provided in Winkler's beam on elastic foundation (BoEF) solution [56]. The solution assumes that the restoring force of the elastic foundation at any point is linearly proportional to the deflection at that point [57]. The BoEF model is therefore analogous to a beam sitting on an infinite system of independent springs. The geometry for Winkler's BoEF with an included adhesive layer thickness is shown in Fig. 15. While Dillard et al. have shown that a sixth-order solution is more accurate for nearly incompressible foundations, such as a soft elastomer like a TPU [57, 58], to account for the finite width of the beam and simplify the boundary conditions

needed for a solution, a fourth-order elastic foundation model was used to approximate the energy release rate.

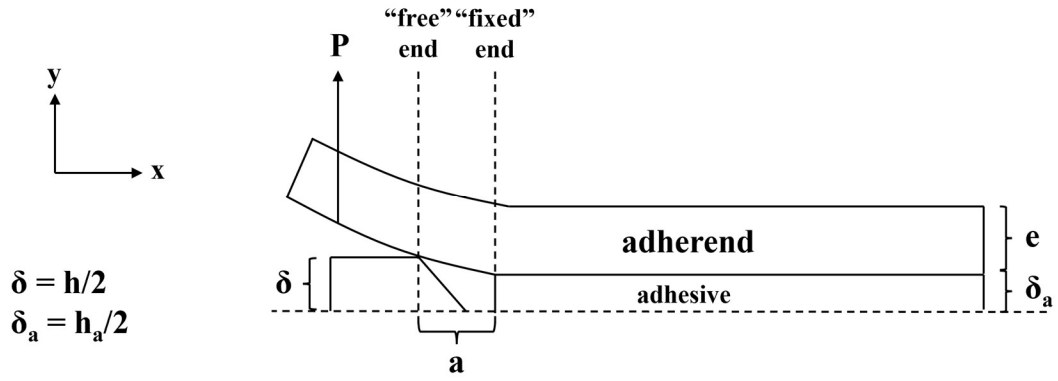

Fig. 15: Geometry of wedge test sample as beam on elastic foundation.

As the crack of the wedge sample grows, two separate regions can be considered along its length. In the region of the sample through which the crack has propagated, there are no surface tractions across the fracture plane, and thus there is no elastic foundation. In the region of the sample still held together by the adhesive, the beam on elastic foundation model can be employed. This will result in the following system of differential equations for the deflection of the beam.

$$\begin{aligned} 0 < x < a: &\quad \frac{d^4 y_1}{dx^4} = 0 \\ a < x < l: &\quad \frac{d^4 y_2}{dx^4} + 4\lambda^4 y_2 = 0 \end{aligned} \tag{26}$$

where y is the vertical deflection of the beam along some horizontal distance x. In Eq. (26), λ accounts for the elastic foundation of the beam present when x is greater than the crack length [57] and is defined as follows.

$$\lambda = \sqrt[4]{\frac{k}{4EI}} \tag{27}$$

where k is the elastic foundation stiffness and is estimated as

$$k = \frac{wE_a}{\delta_a} \tag{28}$$

where E_a is the Young's modulus of the adhesive and δ_a is half the thickness of the adhesive. This equation assumes that the adhesive experiences no lateral coupling (i.e. the restoring pressure is only a function of the displacement at that point rather than being affected by neighboring foundation deflections), and therefore the Poisson's ratio is zero.

Solving Eq. (26) results in the following.

$$0 < x < a: \quad y_1(x) = C_1x^3 + C_2x^2 + C_3x + C_4$$

$$a < x < l: \quad y_2(x) = e^{-\lambda x}[C_5\cos(\lambda x) + C_6\sin(\lambda x)] + e^{\lambda x}[C_7\cos(\lambda x) + C_8\sin(\lambda x)] \tag{29}$$

Defining *y* as the deflection, *y'* as the slope, *EIy''* as the moment, and *EIy'''* as the lateral force exerted on the beam, the following four boundary conditions and four continuity conditions at the point where *x* is equal to *a* can be defined.

Boundary conditions:

$$\begin{aligned} y_1(0) &= \delta - \delta_a \\ EIy_1''(0) &= 0 \\ EIy_2''(l) &= 0 \\ EIy_2'''(l) &= 0 \end{aligned} \tag{30}$$

Continuity conditions:

$$\begin{aligned} y_1(a) &= y_2(a) \\ y_1'(a) &= y_2'(a) \\ EIy_1''(a) &= EIy_2''(a) \\ EIy_1'''(a) &= EIy_2'''(a) \end{aligned} \tag{31}$$

Using Wolfram Mathematica, the system of equations created from the boundary and continuity conditions can be solved for the eight constants in Eq. (29). The applied force along the beam for a specified crack length can then be calculated using the deflections. The lateral force exerted on a beam by the wedge is defined as follows [55].

$$P = EIy_1'''(x) \tag{32}$$

In addition, the compliance for a specified crack length can be calculated using the definitions for the deflection and the force evaluated at the free end of the beam.

$$C = \frac{y_1(0)}{P} \tag{33}$$

These values can then be substituted into the Irwin-Kies equation to solve for the energy release rate, which must then be doubled to account for the two symmetric beams.

The numerical solutions are plotted in Fig. 16. Three curves are drawn with three distinct Young's moduli for the TPU. The energy release rate is greatly reduced in the BoEF solution compared to SBT, especially at small crack lengths, where the differences exceed an order of magnitude. As the crack length reaches the end of the beam, the foundation effect becomes smaller, resulting in more similar behavior between the BoEF solution and the SBT solution. In addition, stiffer materials behave more similarly to the SBT solution, as should be expected.

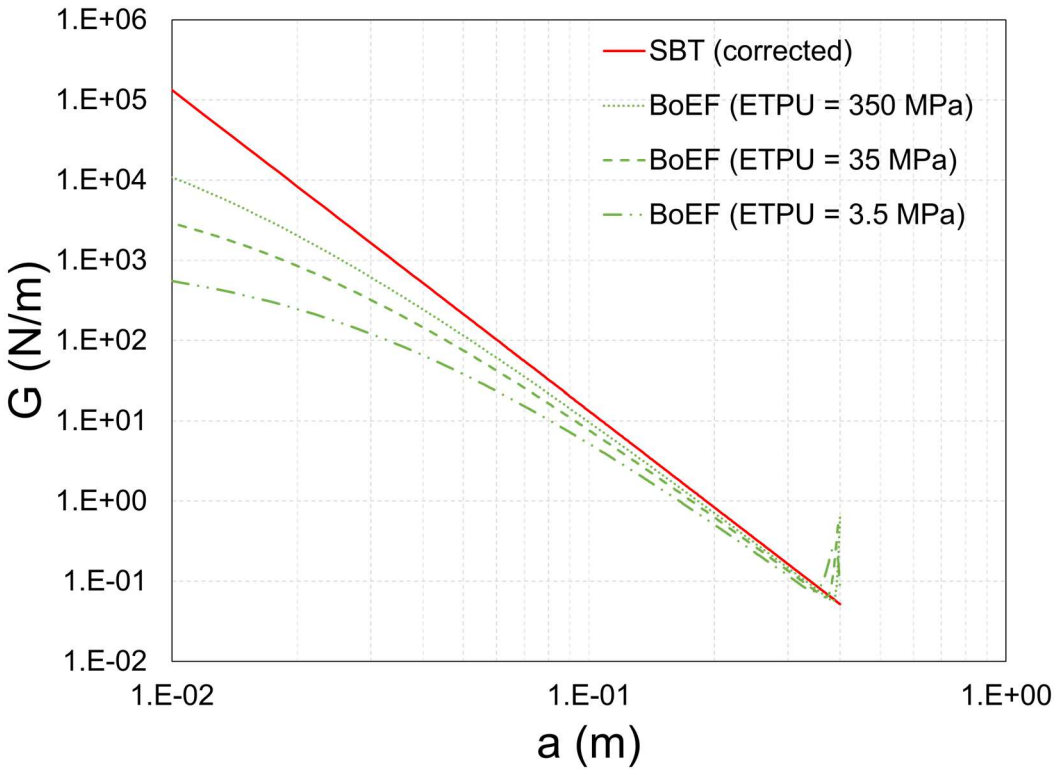

Fig. 16: Comparison of energy release rates for simple beam theory and beam on elastic foundation, at varying elastic moduli

As the crack length approaches the end of the sample and the bond length becomes shorter, significant changes in the energy release rate are observed. Plaut has discussed these end effects for a beam on Winkler and also on an incompressible foundation in [59, 60]. Fig. 17 demonstrates the debonding of a wedge specimen on the end of the sample opposite the wedge. Data in the following sections also show sudden spikes in crack length perhaps attributable to this sudden deflection on the opposite end of the beam. See, for example, the sudden jump in debond length in Fig. 25. In many cases, the wedge specimens fell apart entirely, seemingly driven by debonding from both ends of the beam. The oscillatory nature of the BoEF solution for tractions across the interface suggests that small tensile regions can result at the far end. This, combined with thermal mismatch stresses or other factors, could potentially account for this observation, as could kinetic effects if debonding is rapid.

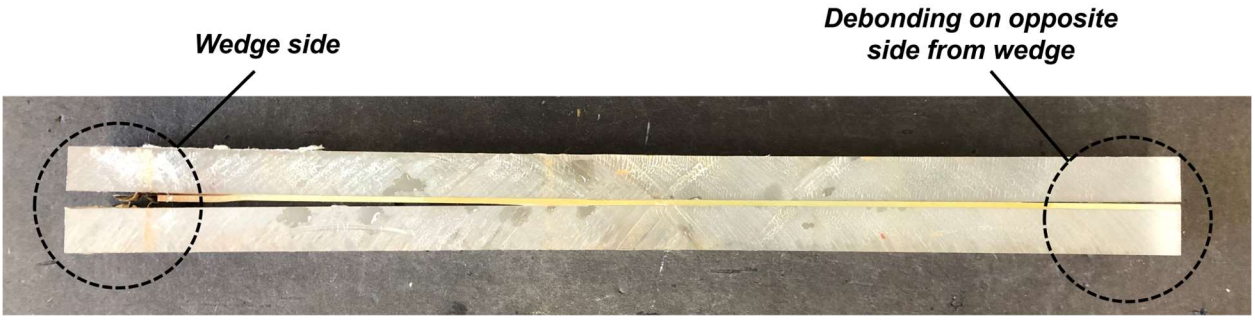

Fig. 17: (EVA 75°C wet) In some of the wedge test samples, the adherends on the side of the sample opposite the wedge began to separate.

As mentioned previously, for BoEF analysis, with the foundation stiffness as assumed in Eq. (28), the Poisson's ratio, v, is essentially equal to zero. This is not, however, the case for the thermoplastic adhesives used in the wedge test, which are nearly incompressible. The fourth-order solution can, nevertheless, be used as an approximation if the material properties are adjusted accordingly.

A three-dimensional finite element analysis was employed to calculate the energy release rates obtained from a number of combinations of elastic moduli (beginning at 2.4 MPa and increasing by a factor of 10) and Poisson's ratios of 0 (to be consistent with the BoEF model) and 0.495 (to roughly approximate an incompressible material) [61]. The compliance as a function of crack length was directly calculated by dividing half the wedge thickness, δ, by the reaction force at that location. Corrected beam theory was used to fit those compliance values as a function of crack length. Those fitted compliance values were used to calculate the energy release rate based on the Irwin-Kies equation. For cases in which the adhesive layer Poisson's ratio was zero, the finite element results agreed well with the BoEF analysis, as expected. Substantial differences between the energy release rates determined using the finite element method and the FEA became apparent for cases where the TPUs are considered to have a Poisson's ratio of 0.495, an upper limit for the element type used in the analysis.

The analysis, however, showed that energy release rates calculated from the BoEF analysis with an elastic modulus 10 times larger than the actual material were in good agreement with the FEA when the Poisson's ratio was 0.495. Case [61] has demonstrated this in Fig. 18 (b), in which there is good agreement between the BoEF values (indicated by the dashed line) and the FEA results (indicated by the symbols) when the value of E in Eq. (28) is taken to be 10 times the true value. This semi-empirical adjustment allows the simple BoEF model to be used for nearly incompressible materials. Consequently, subsequent calculated values of energy release rate appearing in this thesis are based on the beam on elastic foundation analysis with the elastic modulus multiplied by a factor of 10. It should be noted, however, that this value is only expected to be usable for the specific geometry and material properties considered herein.

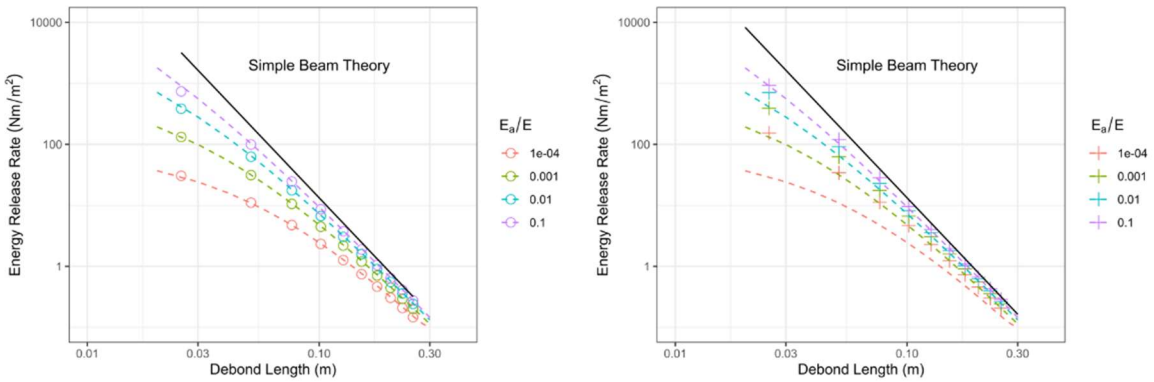

Fig. 18: Energy release rate values found using FEA (symbols), BoEF (dashed lines), and SBT (solid line) at two Poisson's ratios. (Image from [61])

To account for the viscoelastic behavior, a value of the stress relaxation modulus of 2.4 MPa was assumed based on the stress relaxation master curve (so that a value of 24 MPa is used in the calculations for each of the standard TPUs). This is somewhat justified in that Eq. (27) depends on the fourth root of the TPU modulus and is therefore relatively insensitive to the exact value chosen.

3.1.2 Experimental results

The following section provides the experimental results of the wedge tests with analysis based on the previous section. The wedge samples with the three standard TPUs are discussed in section 3.1.3. The stiff TPU is discussed in section 3.1.4. The EVA samples are discussed in section 3.1.5. Wedge samples with potting materials are discussed in section 3.1.6. Wedge samples with edge seals are discussed in section 3.1.7. Finally, surface-treated wedge samples are discussed in section 3.1.8.

In general, each wedge test followed the same initial pattern. The initial straining of the adhesive upon wedge insertion led to what appeared to be rather immediate cavitation in the interlayer for most of the samples. After the initial cavitation, debonding was then observed usually within the first 24 hours of the wedge insertion. Fig. 19 shows the typical pattern observed for the wedge tests with the initial cavitation occurring in the adhesive layer of the samples close to the wedge followed by debonding that extends beyond the cavitation region. In most cases, debonding was observed to grow from the shoulder of the wedge to beyond the cavitation zone, as seen in Fig. 20, which shows cavitation and debonding progression over time within the first twelve hours after the wedge insertion. Fig. 21 gives a graphical depiction of how this pattern of cavitation followed by debonding occurred in both wet and dry samples with TPU #3 at 50°C. The plot shows that debonding was observed in most samples within a day after wedge insertion, with one dry specimen exhibiting no debonding until approximately 10 days after insertion. After debonding occurred, the cavitation typically remained unchanged throughout the length of each test while debonding continued to grow. While the cavitation seems to occur within the interlayer of the wedge sample, the debonding appears to the naked eye to occur at one of the TPU-PC interlayers.

Both the extent of the cavitation and the extent of the debonding were used to make measurements of the overall crack length in the samples, so the following plots refer to the crack length in the y-axis as cavitation/debond length. It should be noted that describing the crack length as both the extent of cavitation and/or debond length has led to some ambiguity in interpretation of wedge test data. This also affects the calculation of the energy release rate, which is based on the crack length, assuming complete debonding rather than cavitation. In future work, it is recommended to distinguish between the two failure modes when measuring the crack growth. While this pattern of cavitation followed by debonding was observed in the majority of the wedge tests, there were some cases where this did not occur. These are pointed out case by case in the following sections.

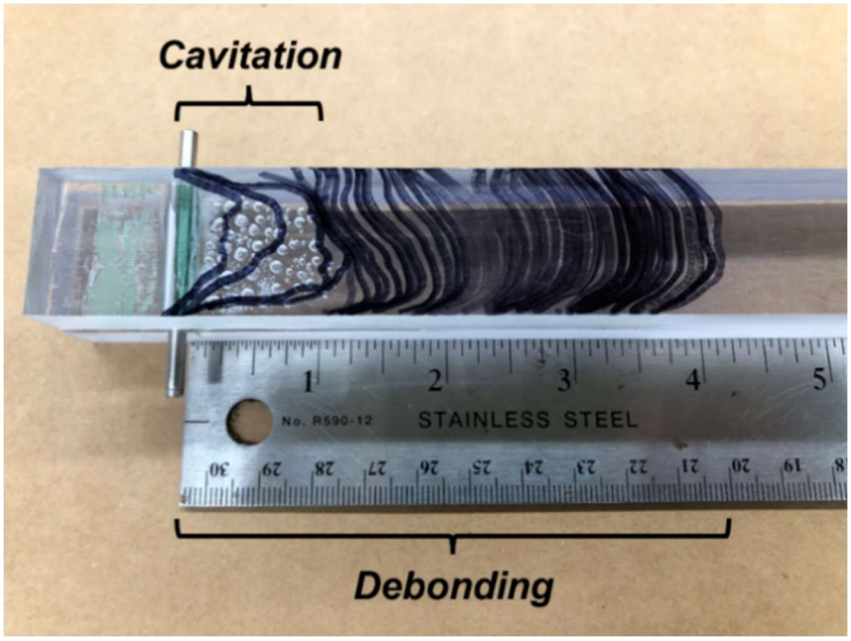

Fig. 19: (TPU #3, 50°C dry) Typical crack growth pattern for the wedge tests. The marker lines indicate the extent of either cavitation or debonding observed at certain times over a period of 290 days. After the wedge insertion, some initial cavitation is observed, seen here from the wedge shoulder to around 1" along the length of the sample. This is followed by debonding, extending from the wedge shoulder (here the contact points on the dowel) to the lengths indicated by the marks on the samples.

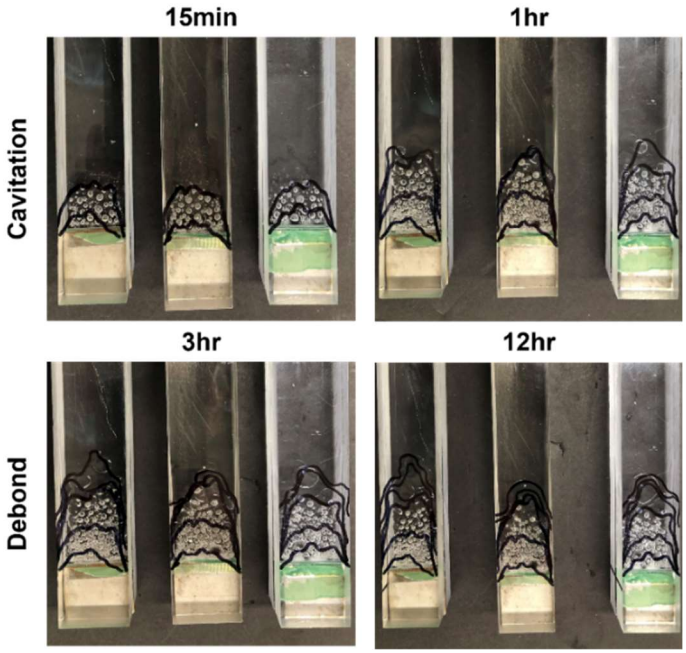

Fig. 20: (TPU #3, 50°C dry) Three replicates indicate the common fracture pattern observed in the wedge tests. 15 minutes after the wedge insertion (top left), cavitation appears near the wedge tip. 1 hour after insertion (top right), the cavitation has grown along the length of the sample. The first debonding is observed 3 hours after the wedge insertion (bottom left) and has continued to grow after twelve hours (bottom right).

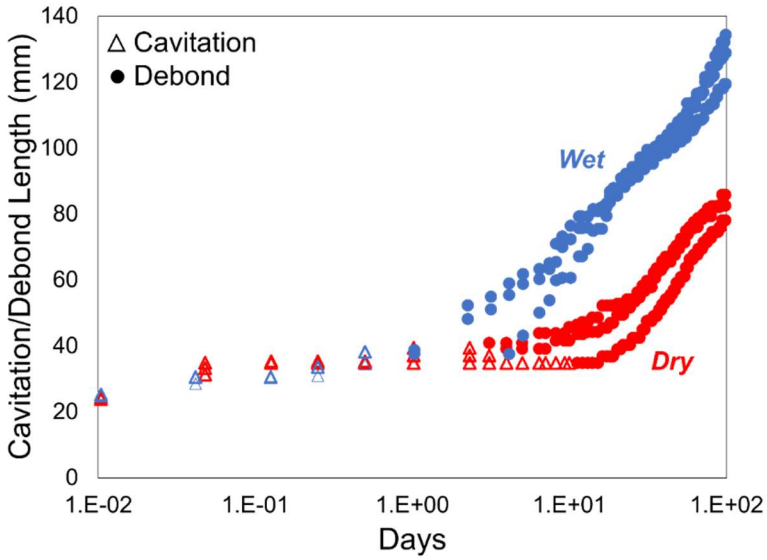

Fig. 21: (TPU #3, 50°C) General pattern observed in wedge samples of initial cavitation followed by debonding. Measurements of cavitation or debond length are shown for three replicates of dry samples and three replicates of wet samples. In most cases, debonding is first observed within the first 24 hours after wedge insertion, except for one dry sample where debonding is not observed until around 10 days.

3.1.3 Standard TPUs

TPU #1, TPU #2, and TPU #3 have been designated as the standard TPUs for this study given their similarities in secant moduli at 100% elongation at room temperature. This section compares the wedge test results for these samples.

Fig. 23 gives the crack length measured as either the extent of cavitation or the extent of debonding plotted against the elapsed time of the test for each of the standard TPUs. The crack lengths are given as averages over three replicates of each test with error bars indicating the largest crack length and the smallest crack length over these replicates. For the standard TPU wedge samples, these error bars are relatively small, indicating little variability among the replicates. This is especially true at shorter times, since the rate of change in the energy release rate with debond length becomes substantially less as the crack length increases, as indicated by the crack length being raised to the negative fourth power in Eq. (25). The increase in variability of measured crack lengths at longer times could reflect this reduced dependence or could be due to the end effects mentioned in section 3.1.1.3 and suggested by Plaut [59, 60].

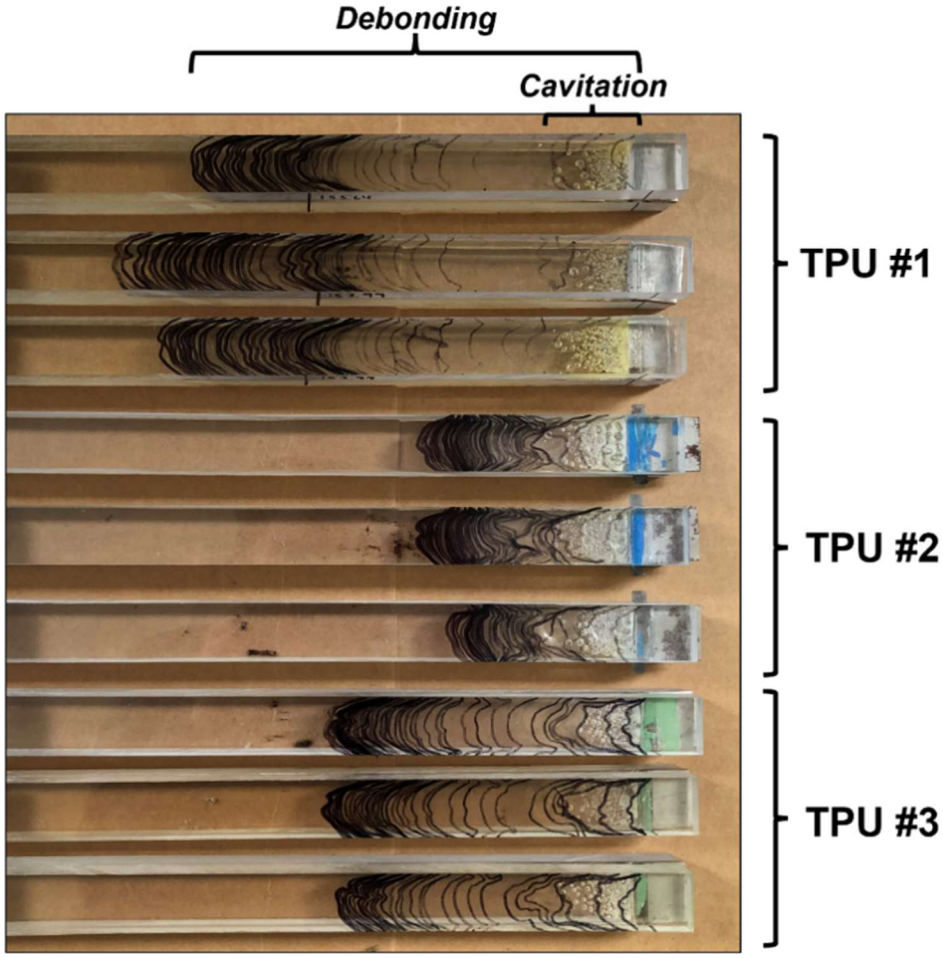

Fig. 22: (75C dry, 300+ days after wedge insertion) Three replicates of each standard TPU held at the same testing conditions are shown here side-by-side. The markings on the samples indicate the cavitation or debonding marked over time. The standard TPU wedge samples followed the typical pattern of initial cavitation followed by debonding.

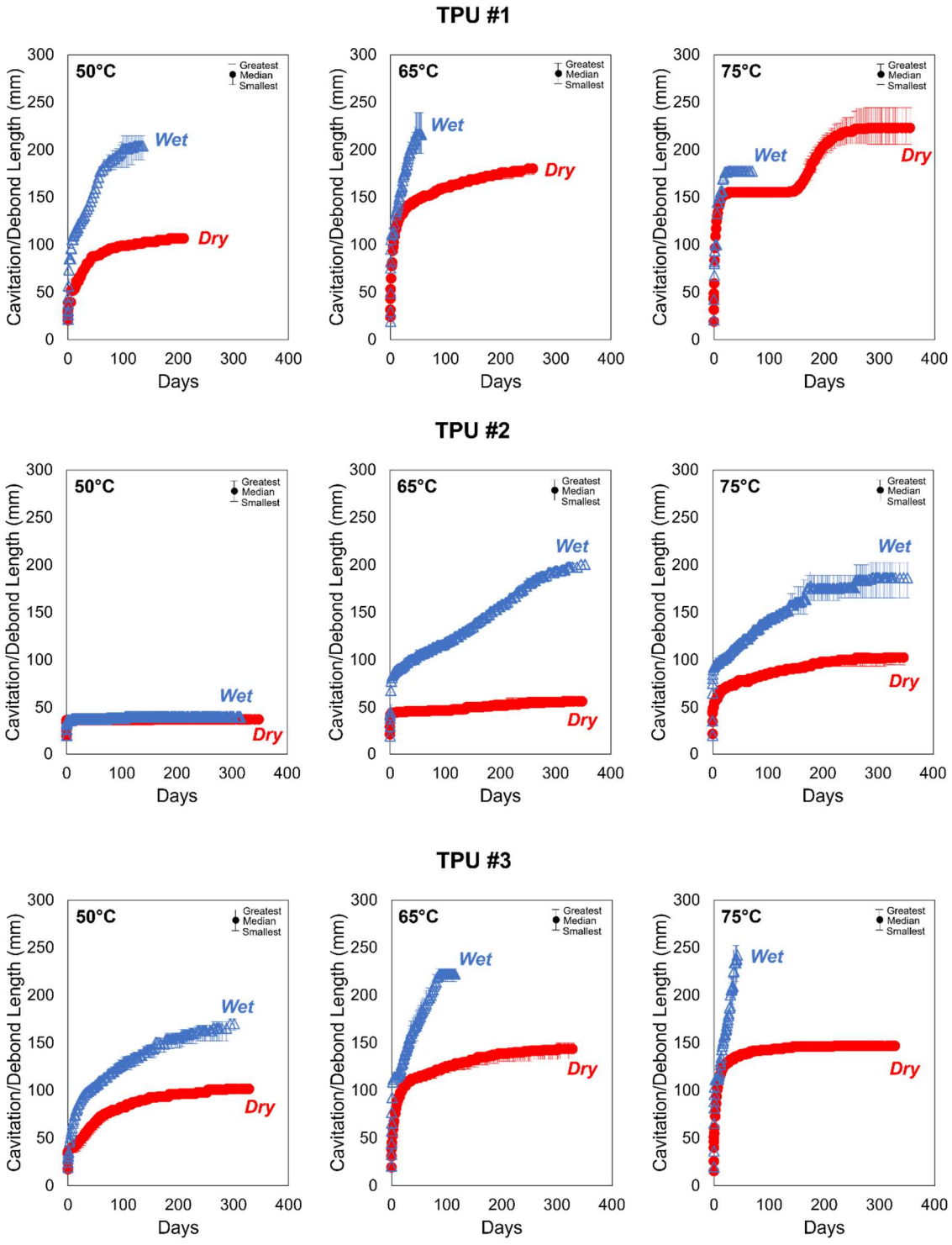

Fig. 23: Crack length versus time plots for standard TPU wedge tests. Crack length is shown here on the y-axis as either the extent of cavitation or debonding measured in the sample. In each plot, the median of three replicates is shown with error bars indicating the greatest and smallest measured crack lengths for that test.

In general, higher temperatures and wet conditions led to higher crack lengths in the standard TPU wedge tests. The samples typically followed the pattern of initial cavitation after the wedge insertion followed by debonding. The only exceptions to this were the 50°C dry and wet samples with TPU #2, in which only cavitation was observed with no debonding. For each of the other samples, interfacial debonding occurred after the initial cavitation. In many cases, this debonding was observed alternating between the two adherends, a phenomenon known as bridging [62-65]. Mukherjee notes in [64] that this effect may be caused by differences in peel strength at different parts of the interface and states that this is an undesirable failure mode for manufacturing applications, and complicates experimental analysis. The bridging effect in the wedge tests is seen in Fig. 24.

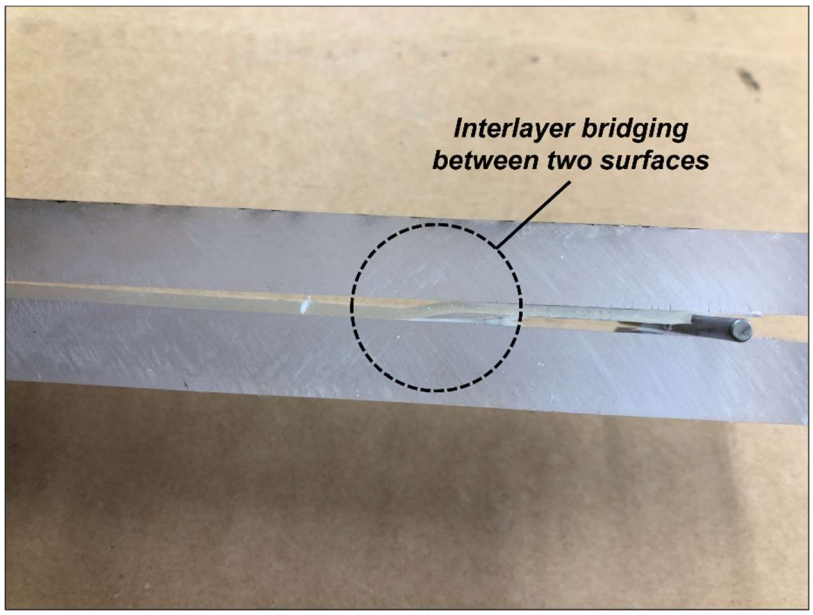

Fig. 24: (75°C dry, TPU #1) In many of the wedge test samples, delamination occurred on both interlayer-adherend surfaces with the two surfaces connected by a bridge formed by the interlayer.

The durability of the standard TPUs is compared simply by overlaying the cavitation/debond length vs. time plots, as in Fig. 25. In general, TPU #2 appears to be the best performing interlayer for the standard TPU wedge tests, producing the smallest crack lengths across each temperature and humidity condition. TPU #1 appears to perform the worst in most cases.

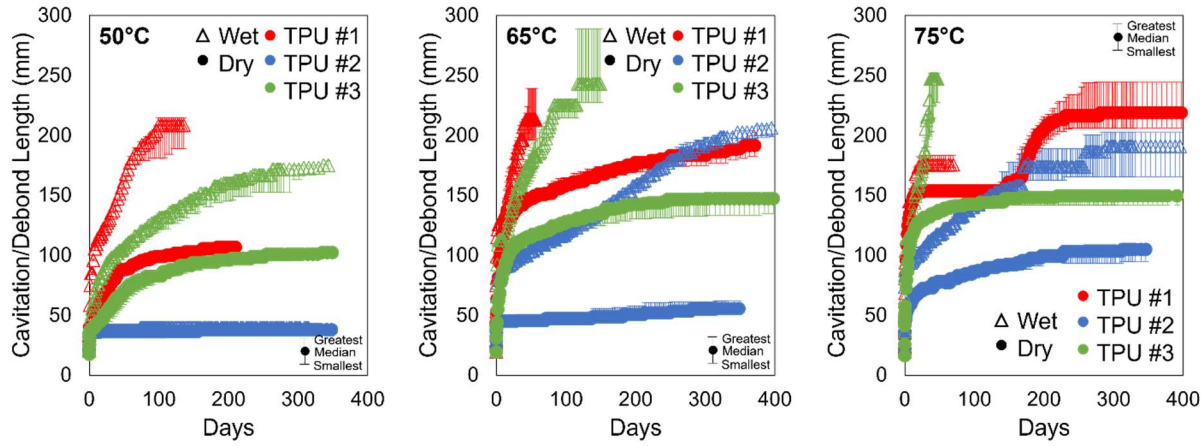

Fig. 25: Overlaid crack length versus time plots of standard TPUs. As in the above figures, the median of three replicates is shown with error bars indicating the greatest and smallest measured crack lengths for that test.

As discussed in the previous section, the evolution of the applied energy release rate, G, is a useful metric in analyzing the fracture resistance of a wedge specimen over time during environmental exposure. Methods for calculating G were discussed in the previous sections. These included simple beam theory (SBT) and Winkler's beam on elastic foundation (BoEF) method, as well as the correction needed to account for the non-negligible thickness of the interlayer. Fig. 16 compares these methods by plotting the crack growth rate versus G for one of the wedge tests using TPU #3 and held at 75°C and dry conditions. The graph indicates significant variance between the different methods. The blue markers indicate G calculated using Eq. (24) in which SBT is used without accounting for the thickness of the adhesive (h_a). The red markers indicate G calculated using Eq. (25) in which SBT is used, but corrections for the effective opening displacement are included. The calculated G values from SBT differ significantly from one another. The purple markers indicate G calculated using BoEF before any correction for material properties based on the FEA has been made. As mentioned, a placeholder of 2.4 MPa for the elastic modulus of the TPU is used. The green markers indicate G calculated using BoEF with an elastic modulus that has been adjusted using the methods described previously using FEA to account for both the compliance and viscoelasticity of the TPU. As mentioned previously, the corrected elastic modulus for this specific wedge specimen is 24 MPa.

Various methods are used in calculating the crack growth rate, *da/dt* [66]. In the following plots, it is calculated using the average crack growth over a certain time period, as shown.

$$\left.\frac{da}{dt}\right|_i \approx \frac{a_i - a_{i-1}}{t_i - t_{i-1}} \tag{34}$$

where a is the measured crack length and t is time. Time periods in which no crack growth was recorded are eliminated from the calculation, so the averages may be taken over different time periods for different crack growth rates.

In general, as time increases the crack growth rate decreases, so data in Fig. 26 was collected top right to bottom left as time progressed. At these early times, indicated by the data points at the top

right of each plot, the energy release rates calculated using BoEF differ by an order of magnitude from the values calculated using SBT. As time goes on and the crack growth rate decreases, however, the values become more similar and are within an order of magnitude.

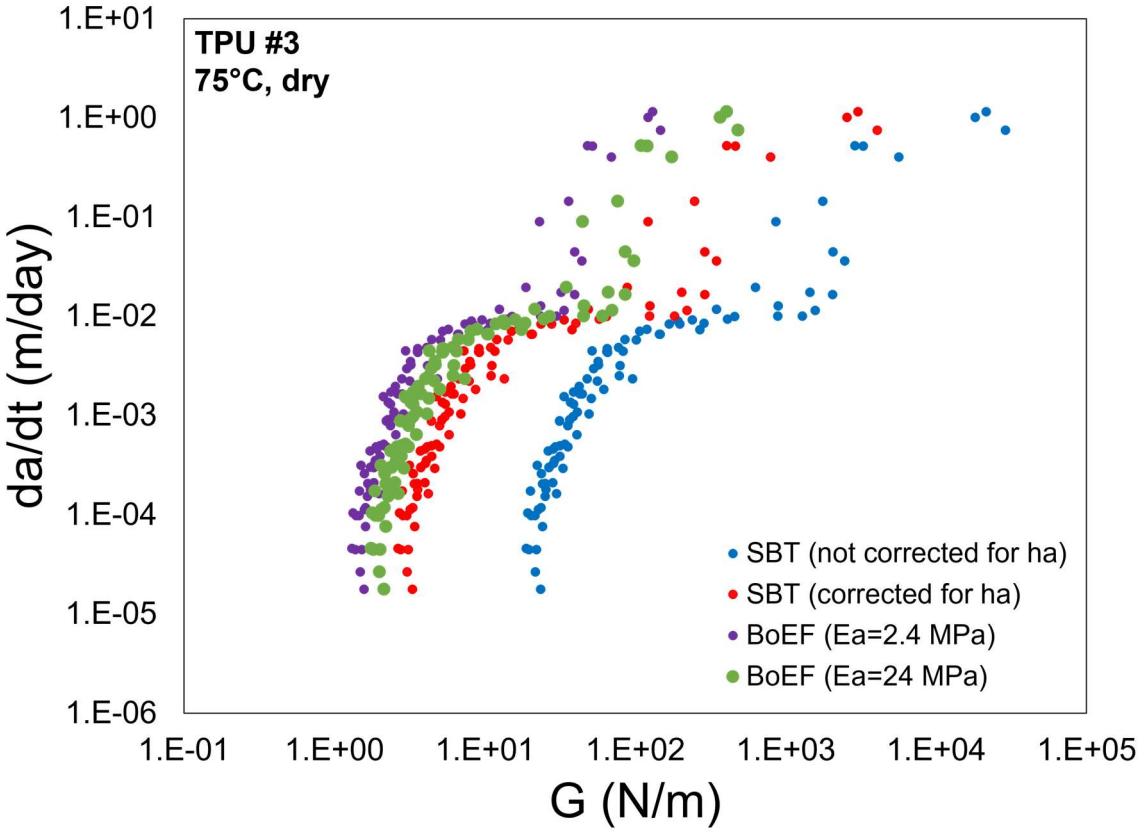

Fig. 26: Comparison of methods for calculating energy release rate. Crack growth rate data is given for three replicates of wedge specimens with TPU #3 held at dry conditions and 75°C.

Fig. 27 compares the energy release rates calculated for each of the standard TPUs at the three different test temperatures using the BoEF method. The elastic modulus used for each TPU is 24 MPa, for the reasons described in section 3.1.1.3.

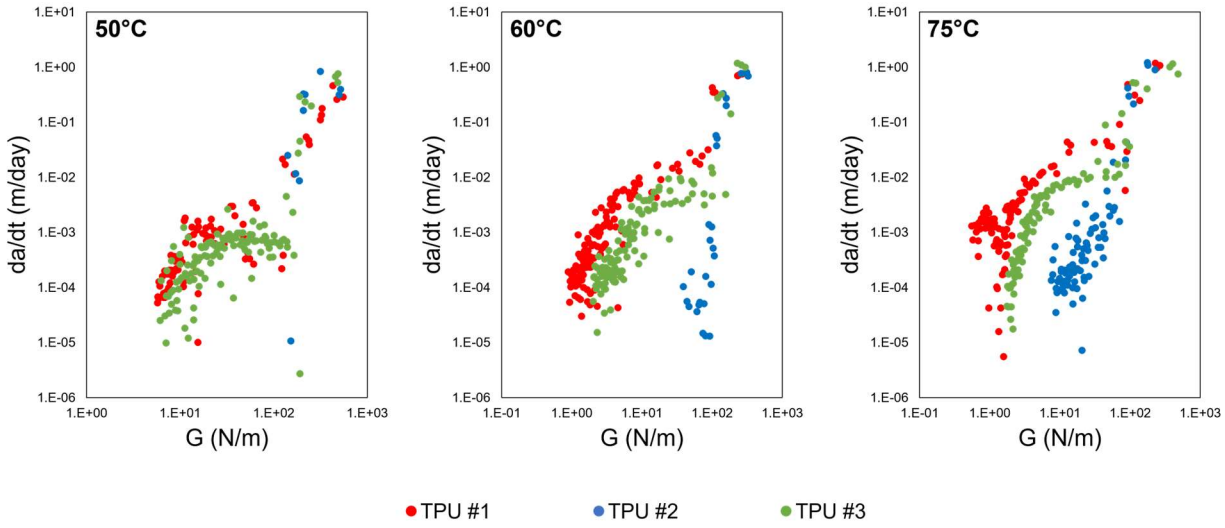

Fig. 27: (Standard TPUs, dry). Crack growth rate plotted against the energy release rate as calculated using the BoEF method for each of the standard TPUs at three different temperatures.

For each of the standard TPUs, at the early times indicated by the data points at the top right of each plot, the energy release rates are very similar. As the crack length increases over time, however, the applied energy release rates drop. Since the energy release rate is inversely proportional to the fourth power of the crack length, the systems with smaller crack growth will have a larger energy release rate. In general, the samples with TPU #2, which exhibited the least debond growth during the wedge tests, maintained the highest energy release rate as the crack growth decreased. Correspondingly, samples with TPU #1 (the worst performing standard TPU) had the lowest energy release rates.

The 75˚C plot in Fig. 27 highlights some challenges with TPU #1, which appears to have an increase in crack growth rate at smaller energy release rates. This is due to the double plateau effect observed in the dry samples of TPU #1 in the 75°C plot (top right) in Fig. 23. After reaching a plateau in which the crack length spent almost a hundred days without any growth, there was then a spike in the crack growth until it reached a second plateau. This plateau could possibly be due to the viscoelastic nature of the TPU as it approaches its hard phase softening point as the time increases. These viscoelastic effects are explored in a later section. The error bars indicate that this is not the result of a single outlier but of all three replicates increasing in crack length at the same time, for reasons not understood at this time. These are the only samples for which this phenomenon occurs, not only for the standard TPUs but across all wedge tests conducted for this thesis, and it continues to be explored.

Overlaying the dry data presented in Fig. 27 with the wet data further shows the decrease in energy release rate as the crack growth increases in the samples. As expected, the calculated energy release rates of the wet samples are lower than the corresponding dry samples as the crack growth rate decreases.

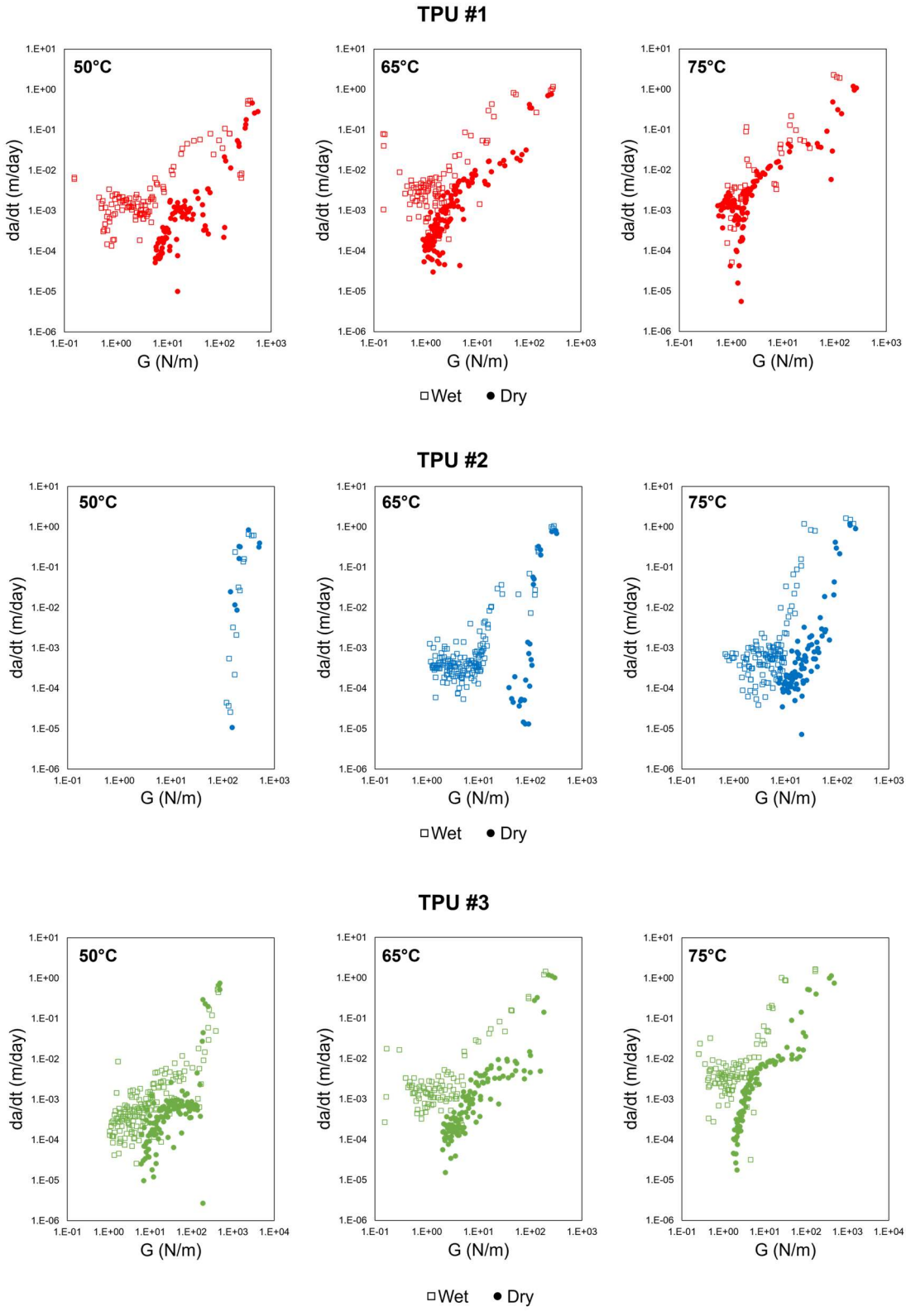

Fig. 28: (Standard TPUs, dry and wet). Crack growth rate plotted against the energy release rate as calculated using the BoEF method for each of the standard TPUs at three different temperatures.

For most of the wedge test samples, the cack growth rate eventually reaches zero and crack length begins to plateau. Evaluating the energy release rate at this crack length could be helpful in characterizing the durability of a material for a given set of conditions. Mueller refers to this threshold value as G_∞ in [67]. While a threshold value is not necessarily reached in the wedge test, G can be reported either when the crack has reached the end of the sample or has stopped growing for an extended time. An example of this is shown in Fig. 29, in which these limiting values of G are calculated for the three standard TPUs when held at 65°C and dry conditions.

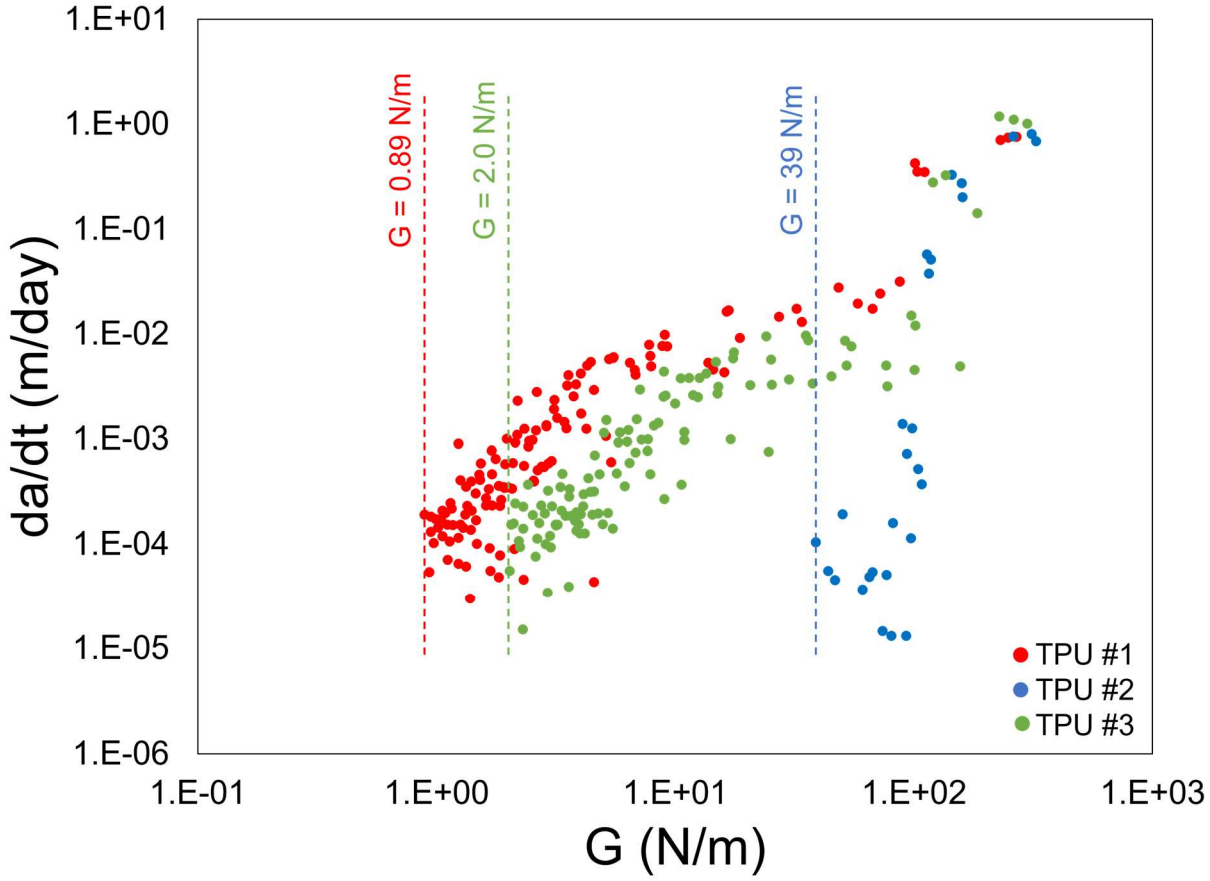

Fig. 29: Limiting energy release rates, G, for each of the standard TPUs at 65°C and dry conditions, due to the crack growth reaching the end of a sample or stopping for an extended time.

3.1.4 Stiff TPU

TPU #4 was designated as the stiff TPU for this study since its secant modulus at 100% elongation at room temperature is nearly four times larger than the standard TPUs, as indicated in Table 1. The wedge test samples with the stiff TPU did not follow the common pattern observed in the standard TPU samples of initial cavitation followed by debonding as shown in Fig. 19 and Fig. 20. No debonding was observed in any of the TPU #4 wedge samples for any temperature or humidity. Instead, wedge insertion and environmental exposure seemed to induce cavitation only. Some of this cavitation was observed far away from the shoulder of the wedge and sometimes a single

bubble would appear in the sample with no neighboring bubbles, as was typically seen around the wedge in each of the other TPUs, where cavitation seemed to occur in closely grouped clusters to relieve the very high stresses induced locally by the wedge. An example of this is shown in Fig. 30, where a solitary bubble is observed far away from the cluster of bubbles observed near the wedge.

Fig. 30: Extensive cavitation is observed in a wedge test sample with TPU #4. A solitary bubble has formed along the length of the samples far away from the typical cavitation observed for the wedge tests that forms in a cluster close to the wedge.

Residual stresses and environmental factors such as temperature and humidity can contribute to the creation of voids or cavities in adhesives that are held in confined spaces [68]. While cavitation and debonding follow similar physical processes, differentiating between the two and understanding their relationship to one another has been a challenge [69]. The first consideration for understanding the extensive cavitation observed in the stiff TPU samples was shear lag induced by a thermal mismatch between the adhesive and adherend [70]. Shear lag refers to a non-uniform stress distribution leading to an increased residual stress. Volkersen provided an analysis of shear lag in [71] by assuming that the adhesive deforms in shear while the adherends do not, and both the adherends and adhesive are linearly elastic. The following differential equation was proposed.

$$\frac{d^2\tau}{dx^2} - \omega^2\tau = 0 \tag{35}$$

where τ is the shear stress, x is the length of the beam, and ω is the reciprocal of the characteristic shear lag or Volkersen length and is defined as follows.

$$\omega = \sqrt{\frac{G}{h}\frac{2}{Ee}} \tag{36}$$

where G is the shear modulus of the adhesive, h is the thickness of the adhesive, E is the elastic modulus of the adherend, and e is the adherend thickness.

Due to the time and temperature dependence of the materials, several Volkersen lengths can be calculated using Eq. (36) for different modulus values of the adhesive and corresponding modulus values for the polycarbonate adherend. Approximate values for the storage moduli are given in Table 3, as obtained by DMA temperature sweeps at a constant frequency. As mentioned previously, for TPUS, the storage modulus is assumed to be equal to the complex modulus obtained from the DMA, as the loss modulus is approximately zero. This approximation is validated by the relatively small tan δ values seen in Fig. 45. Assuming the adhesives are nearly incompressible ($\nu = 0.5$), the shear modulus of the adhesive is assumed to be one third of its storage modulus at that temperature [55].

Table 3: Storage moduli and shear moduli for TPU #4 and PC at wedge test temperatures obtained from dynamic mechanical analysis.

Temperature (°C)	Adhesive E' (MPa)	Adhesive G (MPa)	Adherend E' (GPa)
50	4.4	1.5	2.0
65	3.7	1.2	1.9
75	2.7	0.9	1.8

In Fig. 31, the Volkersen lengths for the wedge tests are show for temperatures ranging from 35°C to 75°C depending on the modulus values determined at those temperatures using dynamic mechanical analysis. The Volkersen lengths at the testing temperatures of the wedge tests are labeled on the plot.

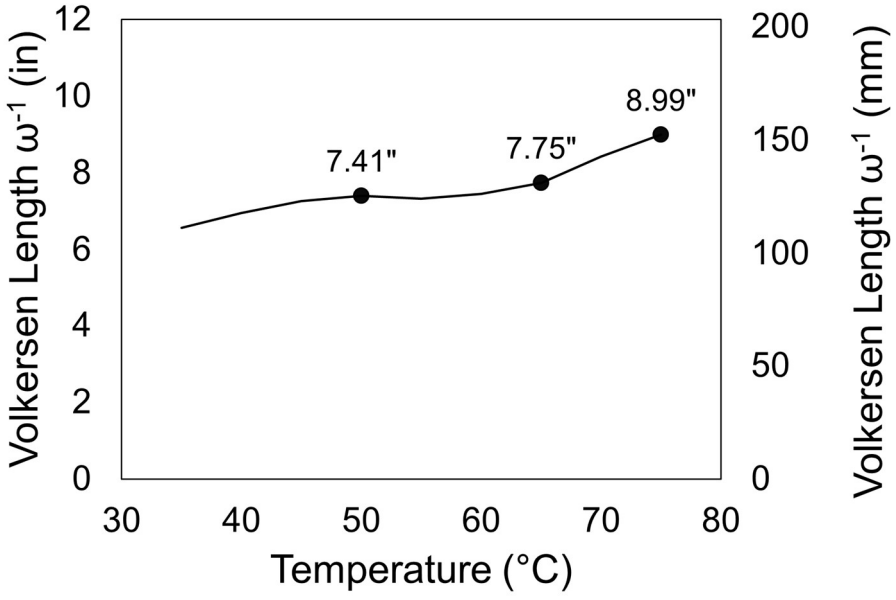

Fig. 31: The calculated Volkersen lengths using DMA values obtained for TPU #4 and PC are plotted with the lengths at the three testing temperatures (50°C, 65°C, and 75°C) of the wedge tests labeled. The large values of the Volkersen lengths, which exceed the width of the samples, indicate that significant residual stress buildup is unlikely.

At each testing temperature, the Volkersen length is well over 1.0", the width of the wedge samples. This indicates that significant residual stress buildup is unlikely across the width of the wedge samples. It should be noted that this does contrast with bonded windows of much larger extent, where there is ample distance to build large in-plane residual stresses within the interlayer. In the case of the wedge test, however, the cavitation observed in the stiff TPU is thus unlikely to be the result of thermal mismatch residual stresses on simple shear lag considerations.

The formation of these isolated bubbles nevertheless indicates the possibility of cavitation due to the environmental conditions. To further explore this possibility, samples with the stiff TPU interlayer with no wedges were placed in the same environmental conditions as the wedge samples. The number of bubbles formed in these samples was observed over time and, as seen in Fig. 32, cavitation was observed that was not driven by the wedge.

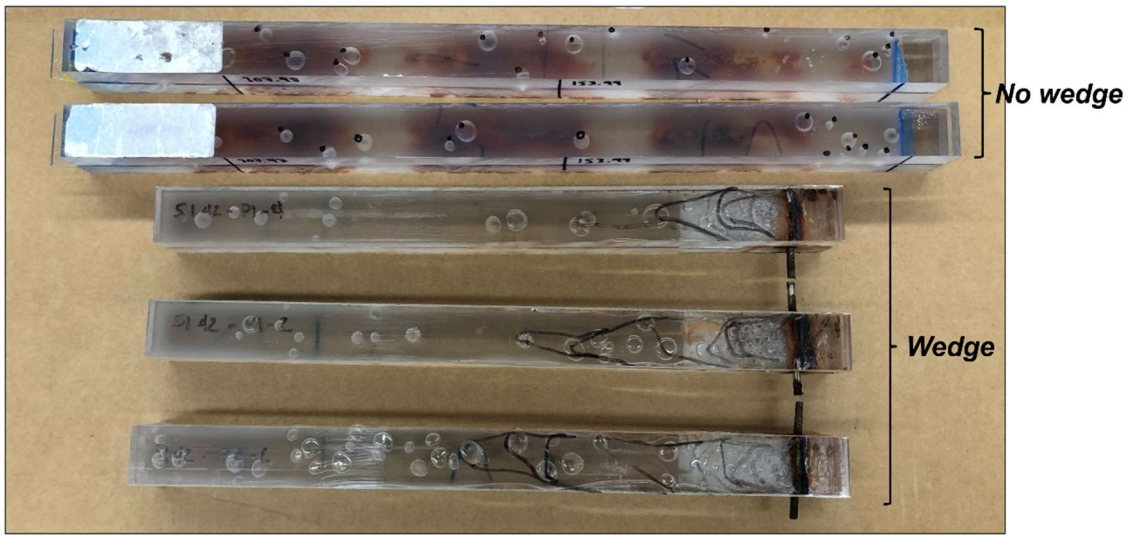

Fig. 32: The top two samples of TPU #4 had no wedge insertion while the bottom three did. Each sample was held at 75°C and wet conditions. Even though there was no wedge insertion for the top two samples, extensive cavitation still forms, indicating that some cavitation formed in the stiff TPU wedge samples was not driven by the wedge.

The addition of cavitation due to a stress driven by something other than the wedge made the crack length measurements and energy release rate calculations for these samples difficult to quantify. It should be noted, however, that the extensive cavitation observed in the stiff TPU samples was not observed in any of the standard TPU wedge tests, other than that found at the crack tip.

3.1.5 EVA

In addition to the TPU interlayers, wedge tests were conducted with samples using an EVA interlayer, another commonly used interlayer for glass laminates, as noted in Section 1.2. In Fig. 33, the results of the EVA wedge test are compared to those of TPU #2, the best performing standard TPU interlayer.

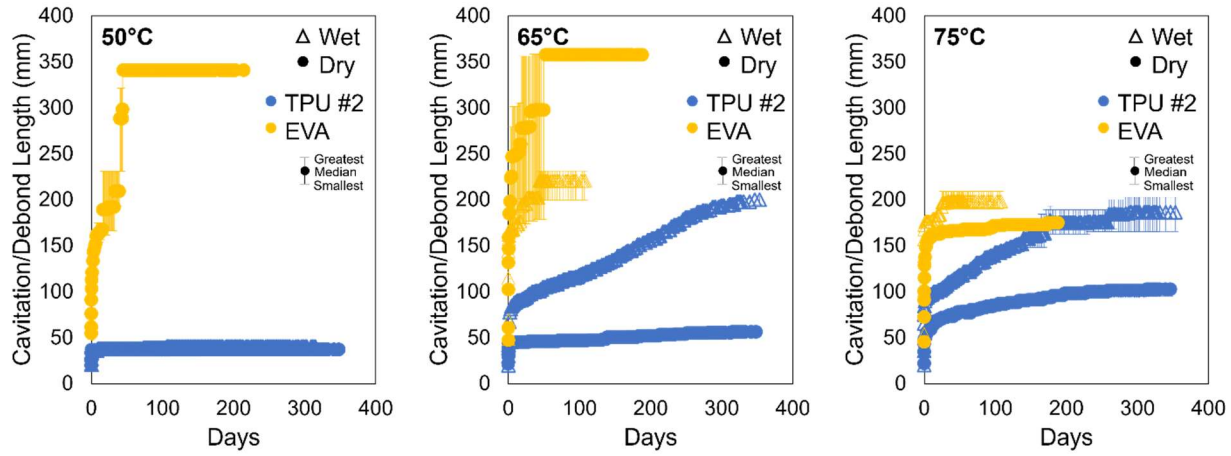

Fig. 33: Crack length versus time plots for EVA compared to TPU #2 (the best performing of the standard TPU interlayers). In each plot, the average of three replicates is shown with error bars indicating the greatest and smallest measured crack lengths for that test. At 50°C, only dry data was collected for EVA samples due to lack of space in water baths.

In contrast to the stiff TPU discussed in Section 3.1.4, no cavitation was observed in the EVA interlayers. Instead, debonding was observed immediately after the wedge insertion. It is clearly seen from Fig. 33 that the EVA wedge samples performed worse than TPU #2, the best performing standard TPU. At lower temperatures, the end effects discussed in section 3.1.1.3 led to the adherends on the end of the wedge sample opposite the wedge to separate much more rapidly than other observed samples. This provides an explanation for the large jumps followed by plateaus observed in the EVA crack length and for the larger crack lengths recorded for the 50°C and 65°C samples compared to the 75°C samples. In future tests, a more accurate measurement would result from recording the crack propagated from the wedge side of the samples and ignoring any debonding from the opposite end.

3.1.6 Potting materials

Three different potting materials were applied to the sides of the wedge samples and underwent the same test procedure as the standard TPU wedge tests. The potting materials are referred to as Potting Material #1, Potting Material #2, and Potting Material #3. Fig. 34 shows the length of either the extent of cavitation or the extent of debonding plotted against the elapsed time of the test for each of the potting materials when applied to a sample with TPU #1, a standard modulus TPU, and compares the recorded crack lengths with those without potting material. The crack lengths are given as the median values over three replicates of each test with error bars indicating the largest crack length and the smallest crack length over these replicates.

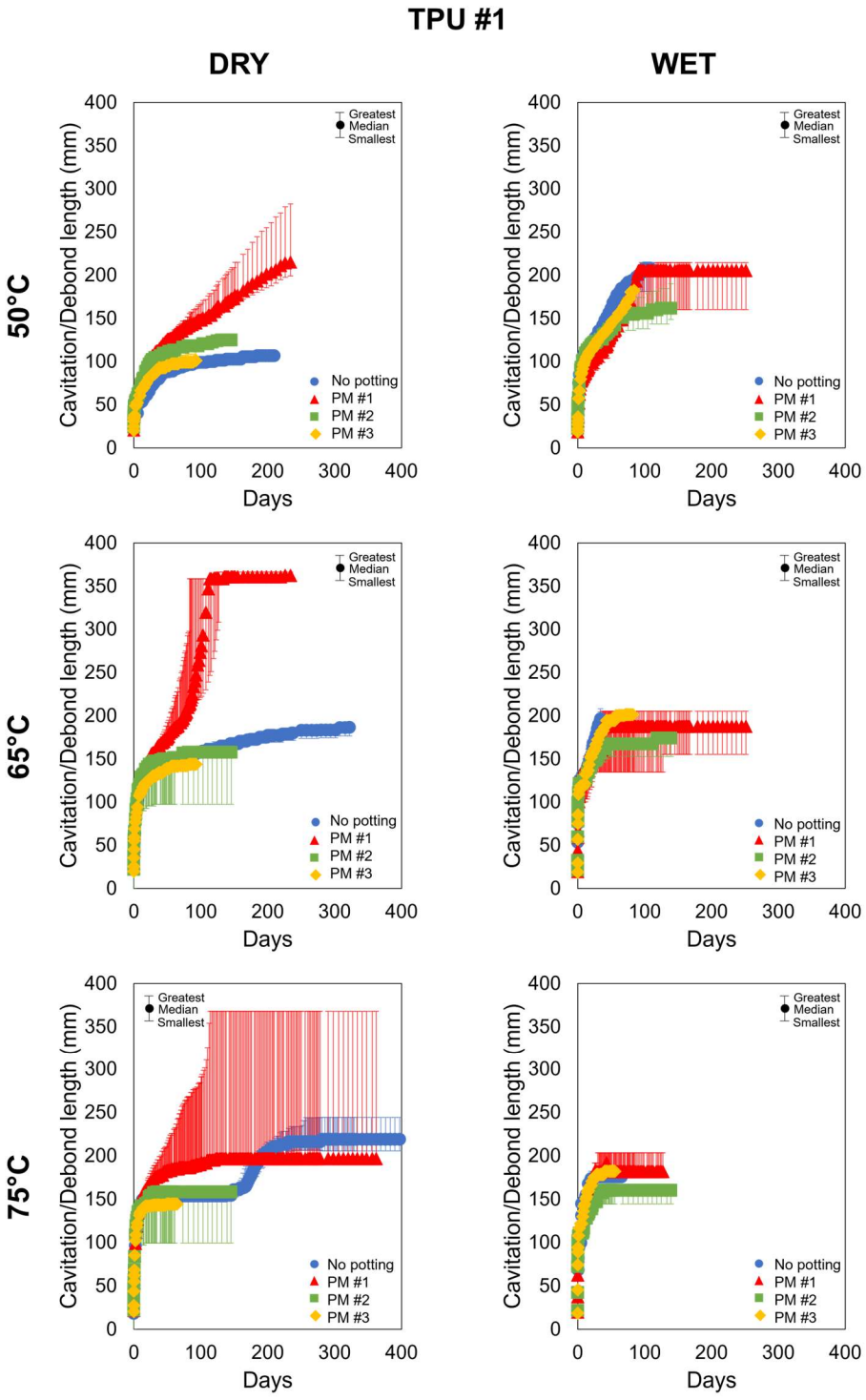

Fig. 34: Crack length vs. time plots for TPU #1 wedge tests with potting materials. Crack length is shown here on the y-axis as either the extent of cavitation or debonding measured in the samples. In each plot, the median of three replicates is shown with error bars indicating the greatest and smallest measured crack lengths for that test.

For the TPU #1 samples, PM #2 and PM #3 do not appear to have any significant effect on the cavitation or debond length. PM #1, on the other hand, appears to negatively affect the crack growth in the dry samples while having little effect on the wet samples. The variability across the three replicates is also very large in the dry PM #1 samples, perhaps indicating that something other than the underlying fracture mechanics is causing the increase in crack growth in the PM #1 samples. For TPU #2 samples, for example, there does not appear to be any significant effect of PM #1 on either the dry or wet samples, as seen in Fig. 35.

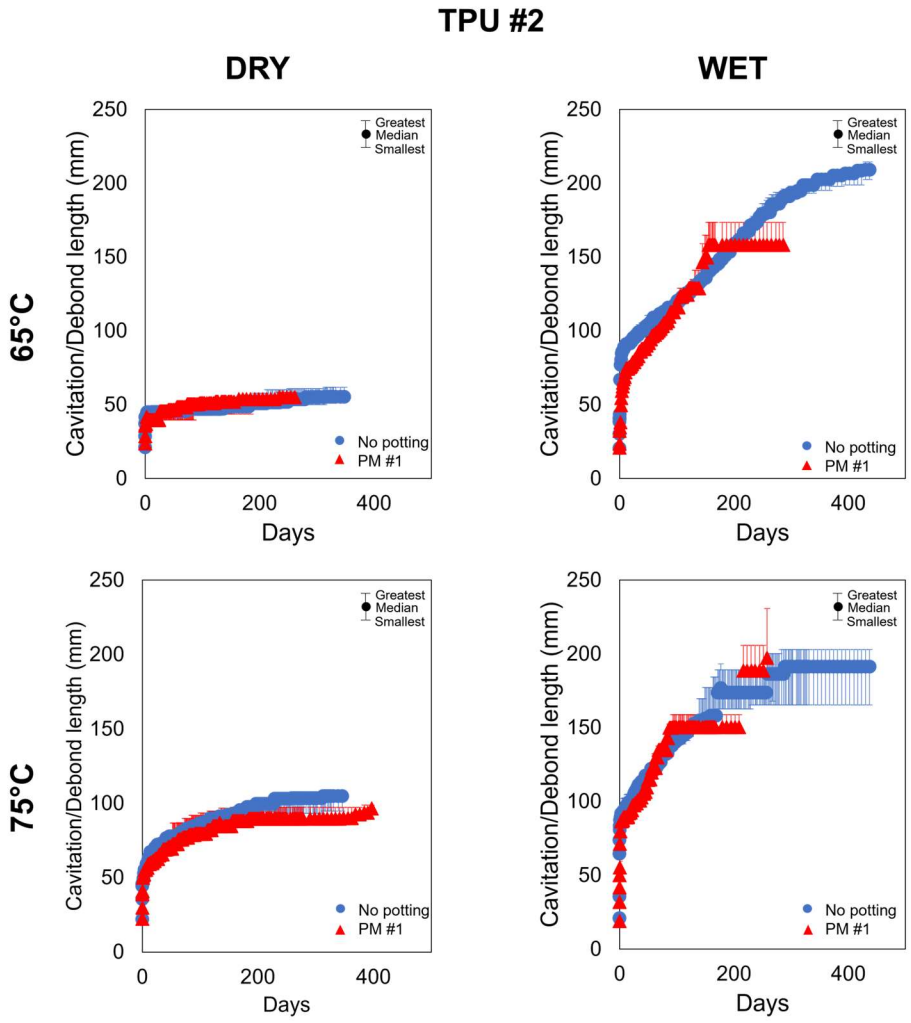

Fig. 35: Crack length vs. time plots for TPU #2 wedge tests with PM #1. Crack length is shown here on the y-axis as either the extent of cavitation or debonding measured in the samples. In each plot, the median of three replicates is shown with error bars indicating the greatest and smallest measured crack lengths for that test. 50°C results are not shown since tests were not conducted on 50°C TPU #2 PM #1 samples due to size constraints of testing ovens.

The lack of change between the PM #1 and no potting material TPU #2 samples indicates that it is unlikely that the potting material is having any degrading effect on the adhesive, as might have been suggested to explain the significant difference in the TPU #1 samples. A possible explanation is that while there could be a degrading effect caused by the interaction of PM #1 and the adhesive,

in the case of TPU #2, this is counteracted by the load carrying capabilities of the potting material. As noted previously, one reason for adding potting material to ballistic glass systems is to provide support to bear the load of any stresses on the system. This could certainly be the case for the wedge tests, where the load bearing nature of the potting material is counteracting any negative degradation it causes.

Various methods were used to further explore the effect of potting material on the durability of the TPUs. Dogbone samples of the 0.025" (0.6 mm) thick TPU films were cut using ASTM D638 [72], resulting in specimens with a gage length of 2.5" (63.5 mm) and width of 0.25" (6.4 mm). The TPU film samples were then hung in a 75°C oven and 500g weights were hung from them to create a tensile creep test. These tests were conducted on six replicates each of TPU #1 and TPU #2. Comparisons were also made between samples that had undergone the autoclave process and those that had not. For each group of replicates, an approximately 0.25" (6.4mm) by 0.35" (8.9 mm) bead of PM #1 with thickness of approximately 0.1" (2.5 mm) was applied to the center of the dogbone sample on either side.

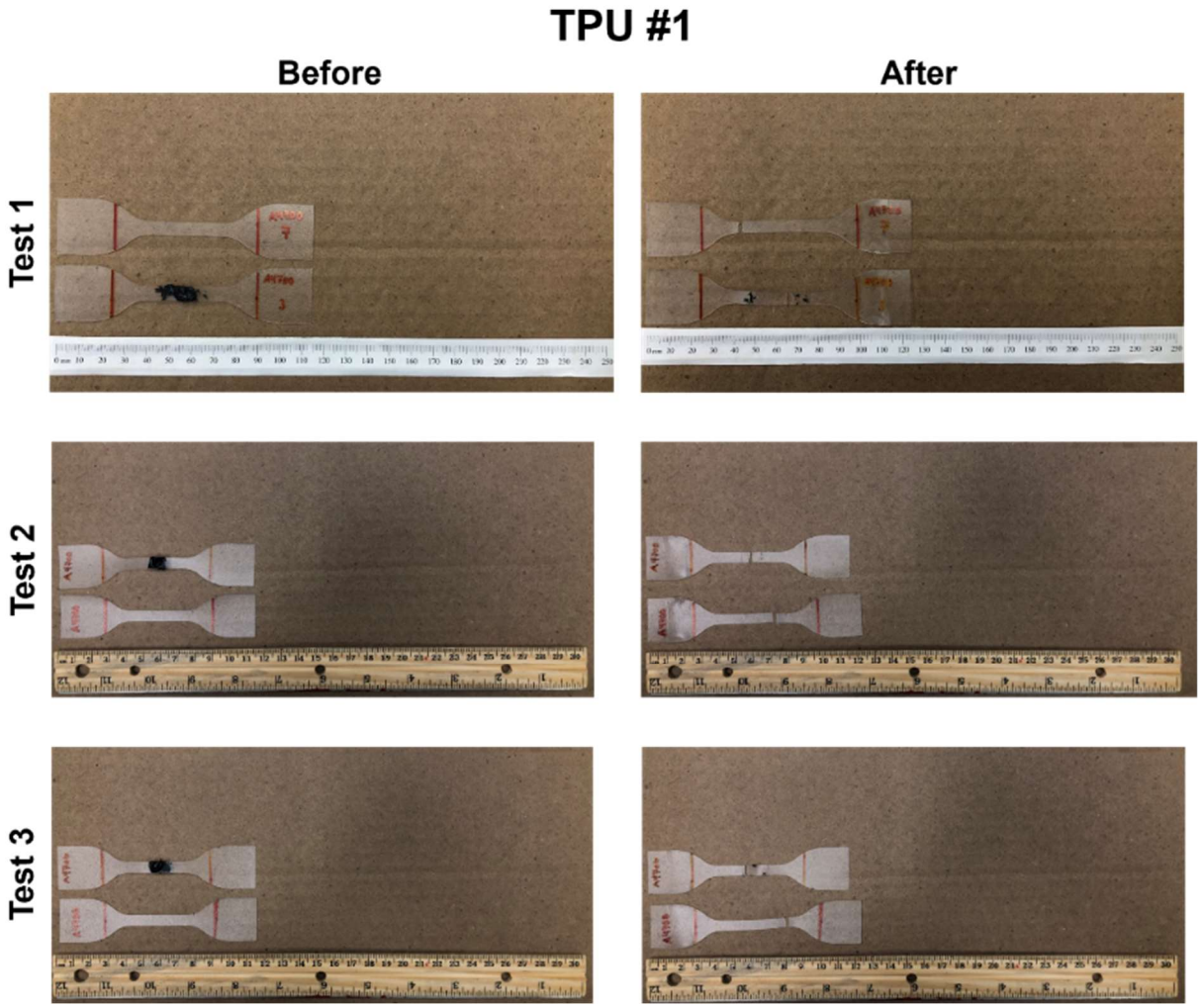

Fig. 36: Tensile creep tests samples for TPU #1 films tested at 75°C with a 500g dead weight. The images show the samples before (left) and after (right) the tests were conducted. In each image, a sample with a bead of PM #1 applied to the center of the sample is compared to a sample with no potting material. For TPU #1, there does not appear to be any significant effect from the addition of PM #1; however, quick, brittle fracture makes it difficult to compare samples with or without potting material.

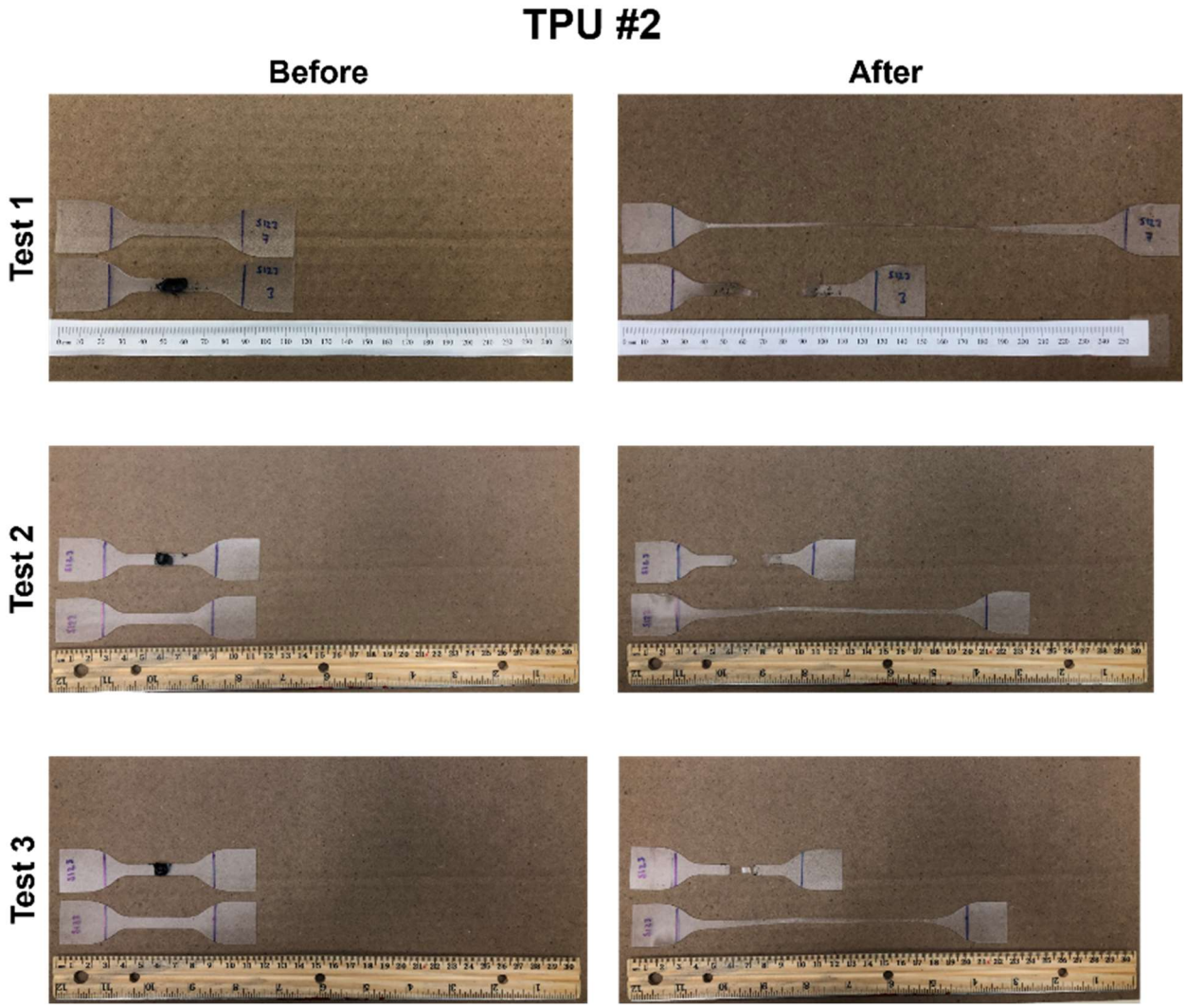

Fig. 37: Tensile creep tests samples for TPU #2 films tested at 75°C with a 500g dead weight. The images show the samples before (left) and after (right) the tests were conducted. In each image, a sample with a bead of PM #1 applied to the center of the sample is compared to a sample with no potting material. For TPU #2 samples, there is a significant change in the strain at fracture of the TPU films with PM #1 applied.

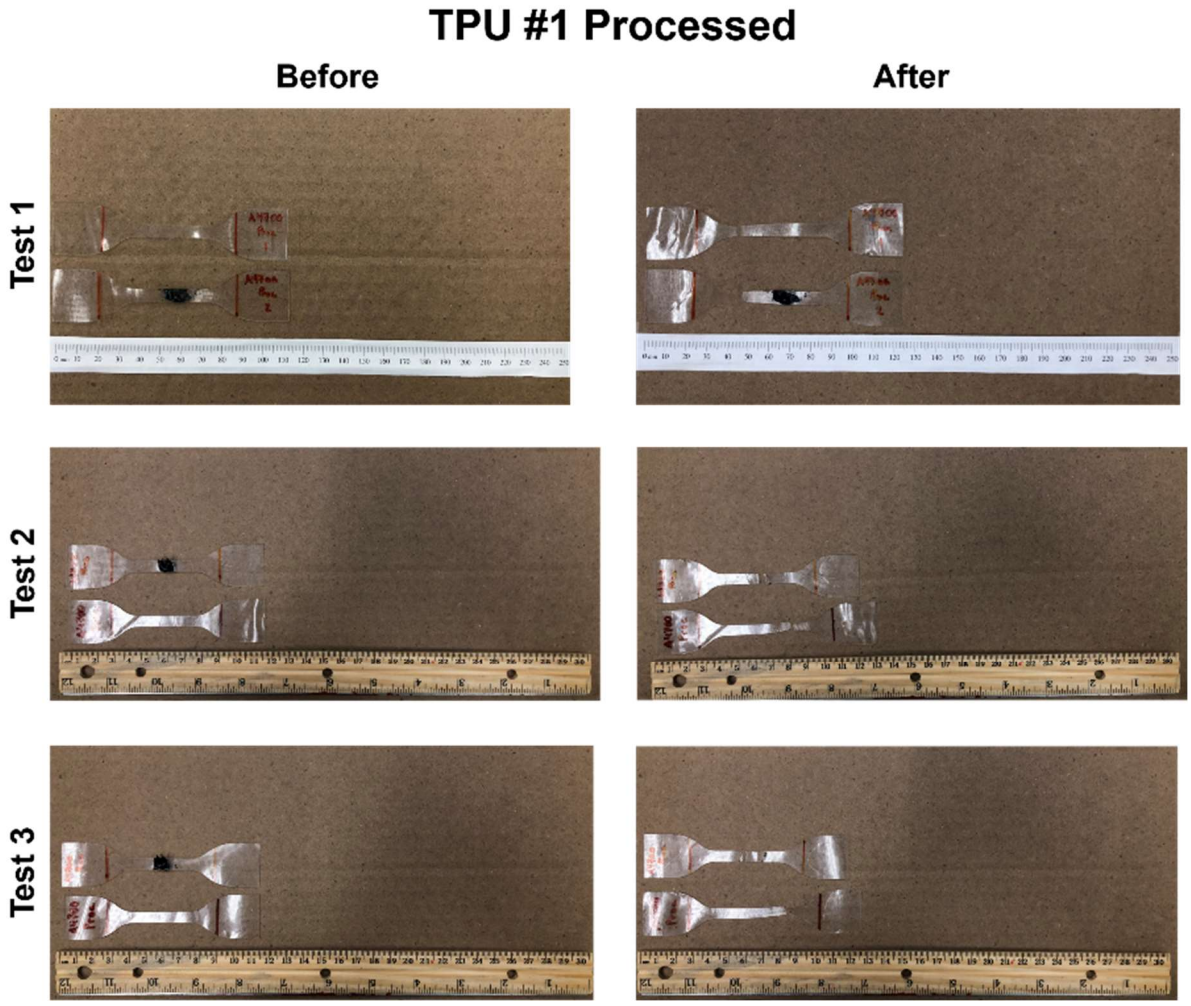

Fig. 38: Tensile creep tests samples for autoclave-processed TPU #1 films tested at 75°C with a 500g dead weight. The images show the samples before (left) and after (right) the tests were conducted. In each image, a sample with a bead of PM #1 applied to the center of the sample is compared to a sample with no potting material. Similar to non-processed TPU #1, there does not appear to be any significant effect from the addition of PM #1.

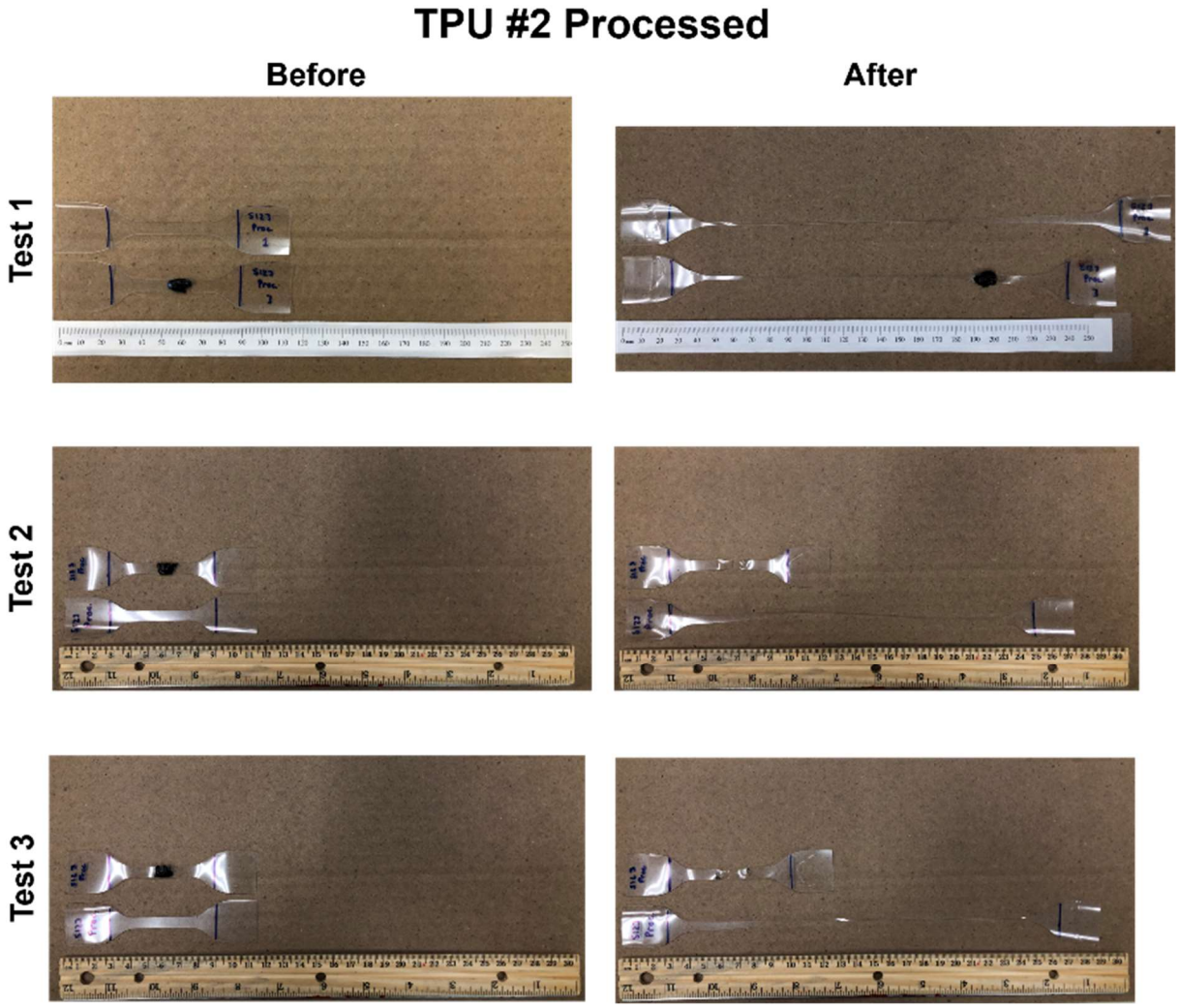

Fig. 39: Tensile creep tests samples for autoclave-processed TPU #2 films tested at 75°C with a 500g dead weight. The images show the samples before (left) and after (right) the tests were conducted. In each image, a sample with a bead of PM #1 applied to the center of the sample is compared to a sample with no potting material. Similar to non-processed TPU #2, there is a significant change in the strain at fracture of the TPU films when PM #1 is applied.

The results from these rather crude tensile creep tests shown in Fig. 36 - Fig. 39 suggest that the presence of PM #1 can result in failures at much lower creep strains for the TPU #2 system. For the creep tests, this effect is obvious in the TPU #2 films, as seen in Fig. 37 and Fig. 39. While the samples with no potting material were extremely ductile for TPU #2, never actually fracturing during the duration of the test, the films with PM #1 appeared to fail in a more brittle fashion, fracturing without substantial creep deformation in most cases. While the effect of PM #1 on the wedge tests was more easily seen in samples with TPU #1, for these creep tests, the effect of PM #1 was less significant for TPU #1. This is likely due to the fact that the stiffness of the TPU #1 film was high even for samples without any potting material applied. This resulted in very quick tests lasting under a minute long that ended in the brittle fracture of all of the TPU #1 samples tested. The results from the tensile creep tests confirm that there is a negative effect caused by the application of PM #1 in some cases, as was seen in some cases for the wedge tests.

3.1.7 Edge seals

As described in section 2.2.2, three different edge seals were applied to the sides of a number of the wedge samples and underwent the same test procedure as the standard TPU wedge tests. The edge seals are referred to as Edge Seal #1, Edge Seal #2, and Edge Seal #3. The number of edge seal samples available for testing was limited to samples with TPU #3, and testing was conducted only for dry samples at 50°C and 75°C. Fig. 40 shows the length of either the extent of cavitation or the extent of debonding plotted against the elapsed time of the test for each of the edge seal samples and compares the recorded crack lengths with those without any edge seal. The crack lengths are given as the median values over three replicates of each test with error bars indicating the largest crack length and the smallest crack length over these replicates.

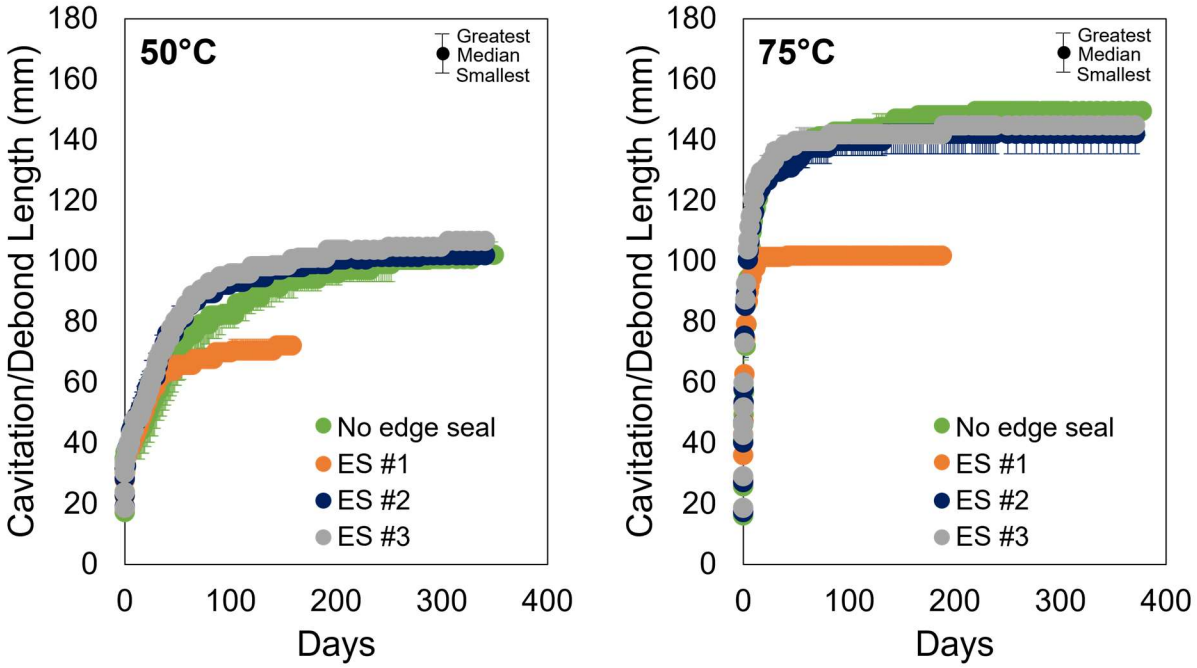

Fig. 40: Crack length vs. time plots for TPU #3 dry wedge tests with edge seals. Crack length is shown here on the y-axis as either the extent of cavitation or debonding measured in the samples. In each plot, the median value of three replicates is shown with error bars indicating the greatest and smallest measured crack lengths for that test. The results indicate that ES #1 has a positive effect on the wedge samples.

The above plots indicate that ES #2 and ES #3 have no significant effect on the crack lengths observed in dry wedge samples with TPU #3. ES #1, however, has a significant positive effect, producing smaller crack growth than samples with no edge seal at both 50°C and 75°C.

To determine whether or not the edge seal is bearing any of the load caused by the stress due to the wedge insertion, a matting knife was used to cut a slit through ES #1 on both sides of the samples along its length. Fig. 41 shows one of these wedge samples after the edge seal has been slit.

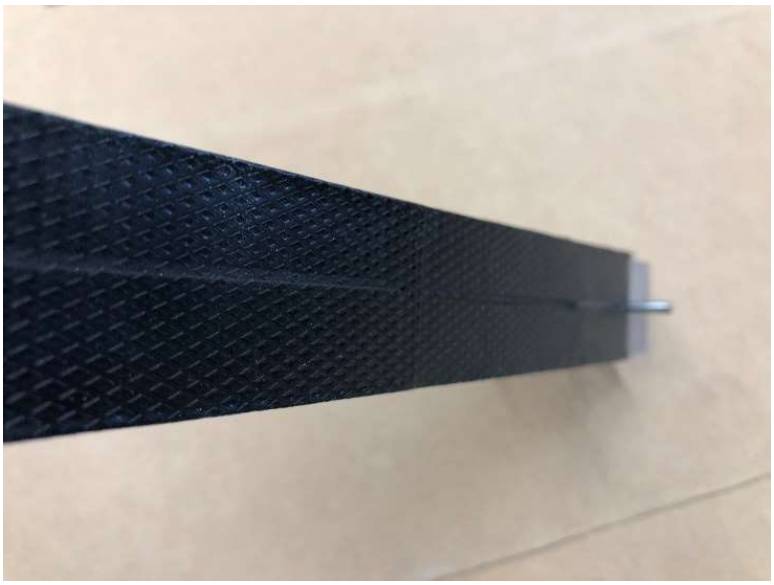

Fig. 41: Wedge test sample after the edge seal has been slit along the length of the sample. Though difficult to see the slit in the image, cutting the edge seal led to an increase in the crack length.

After ES #1 was slit and the samples were returned to their previous testing environments, the crack lengths continued to rise despite having already reached a plateau, as seen in Fig. 42. These results indicate that in the case of the ES #1 wedge samples, the edge seal is bearing some of the load caused by the insertion of the wedge.

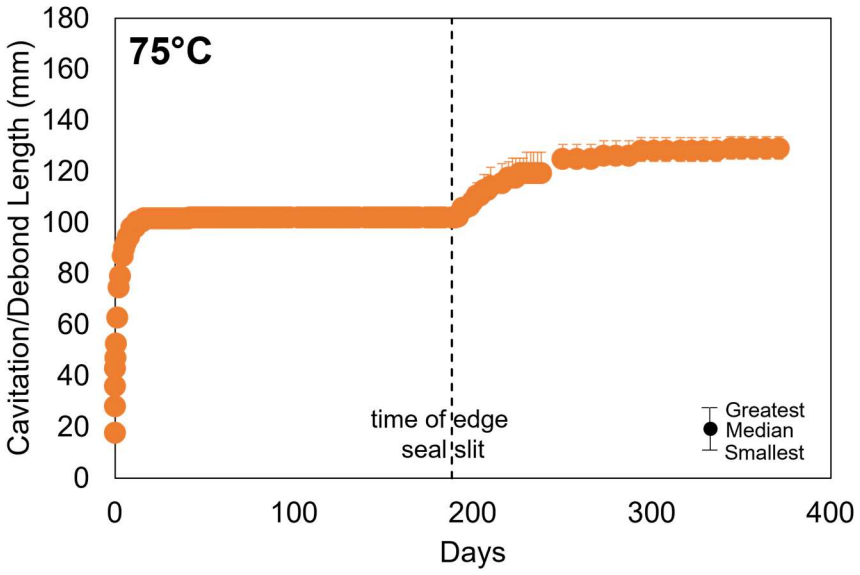

Fig. 42: Crack length versus time plot for TPU #3 75°C dry wedge tests with ES #1. The dashed line indicates the time during the test in which the edge seal was slit on both sides of the sample along its length. Almost immediately after the edge seal is slit, the crack length begins to increase again even though it had already reached a plateau.

After seeing these results from the ES #1, the same method was applied for the ES #2 samples. A matting knife was again used to cut a slit on both sides of the samples along their lengths, and the samples were returned to their previous testing environment. Unlike ES #1, however, no increase in the crack length was observed, as seen in Fig. 43.

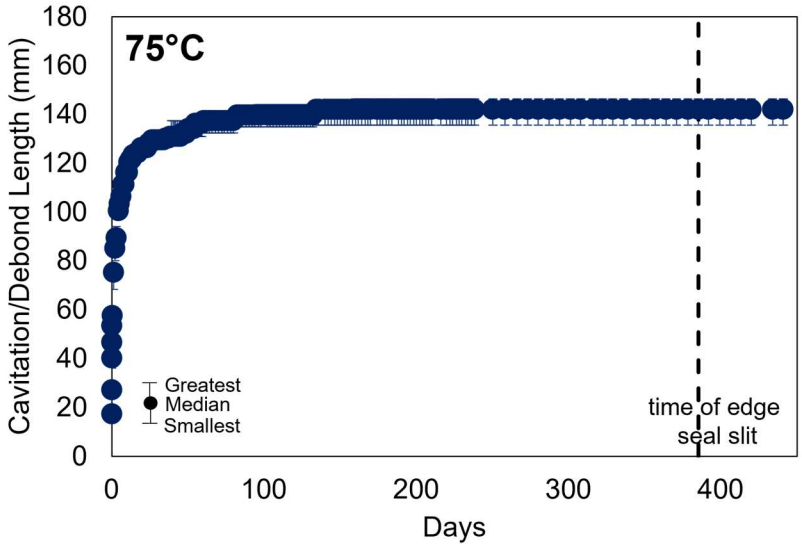

Fig. 43: Crack length versus time plot for TPU #3 75°C dry wedge tests with ES #2. The dashed line indicates the time during the test in which the edge seal was slit on both sides of the sample along its length. Unlike ES #1, there is no change in the crack length after the time of the edge seal slit.

These results indicate that ES #2 is not bearing a significant portion of the load caused by the insertion of the wedge and that ES #1 is a more reliable edge seal in holding the wedge samples together. It should be noted that while the load-carrying capabilities of ES #1 are apparent in the wedge samples, real-life applications like full-sized ballistic resistant windows may not see such an effect since the geometries are so different.

3.1.8 Surface treated samples

The final wedge tests were conducted with surface treated samples with TPU #2. Plasma-treated samples were provided by JNI Armor, and the tests were conducted using the same process as the previous wedge tests and at the same temperatures and humidity conditions. The surface-treated samples did not have any potting material or edge seal applied to them and no specific details were provided regarding the nature of the plasma treatment.

Short-term results indicated that the plasma-treated samples produce smaller crack lengths than non-treated samples for both dry and wet cases across all temperatures, as seen in Fig. 44 below.

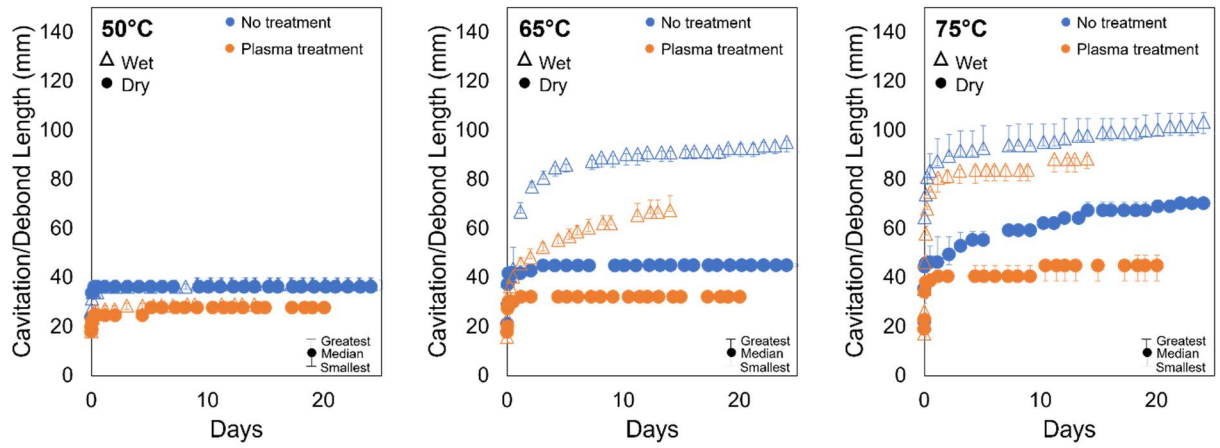

Fig. 44: Crack length versus time plots for plasma-treated samples with TPU #2 compared to non-surface-treated samples. In each plot, the median of three replicates is shown with error bars indicating the greatest and smallest measured crack lengths for that test.

3.2 DMA

3.2.1 Overview

The material properties of thermoplastic polyurethanes are both time and temperature dependent due to their viscoelastic nature. When performing fracture analysis involving these materials properties, it is therefore necessary to have a range of values based on both the frequency of the applied load and the temperature at which it is applied. The DMA results presented in this section, for example, have already been referred to in this thesis in the use of calculating the energy release rate of a wedge specimen. Not only is DMA helpful in providing material properties with which to make calculations, but the material properties themselves are useful in determining how the different TPUs respond to changes in temperature and loading rate.

The following sections report the collection of viscoelastic properties from the dynamic mechanical analysis described in sections 1.5 and 2.3. These results are split into three sections. The DMA results for the three standard TPUs are discussed in section 3.2.2. The stiff TPU is discussed in section 3.2.3. Finally, the DMA results of some remaining TPU and PVB films are discussed in section 3.2.4.

3.2.2 Standard TPUs

The first DMA testing for this study was performed on the standard TPU films described previously (TPU #1, TPU #2, and TPU #3). These TPUs were designated as standard TPUs due to their very similar secant moduli at 100% elongation at room temperature, as seen in Table 1. Despite the similarity in their secant moduli, it has already been shown that the interlayers have very different effects on the wedge test samples. Wedge tests with TPU #2, for example, generally resulted in smaller crack length than TPU #1 and TPU #3. A possible explanation for this difference in performance is the viscoelastic nature of TPU #2. Dynamic mechanical analysis was

used using the method described in section 2.3 to explore this possibility. Fig. 45 shows the overlaid frequency sweeps of the standard TPUs.

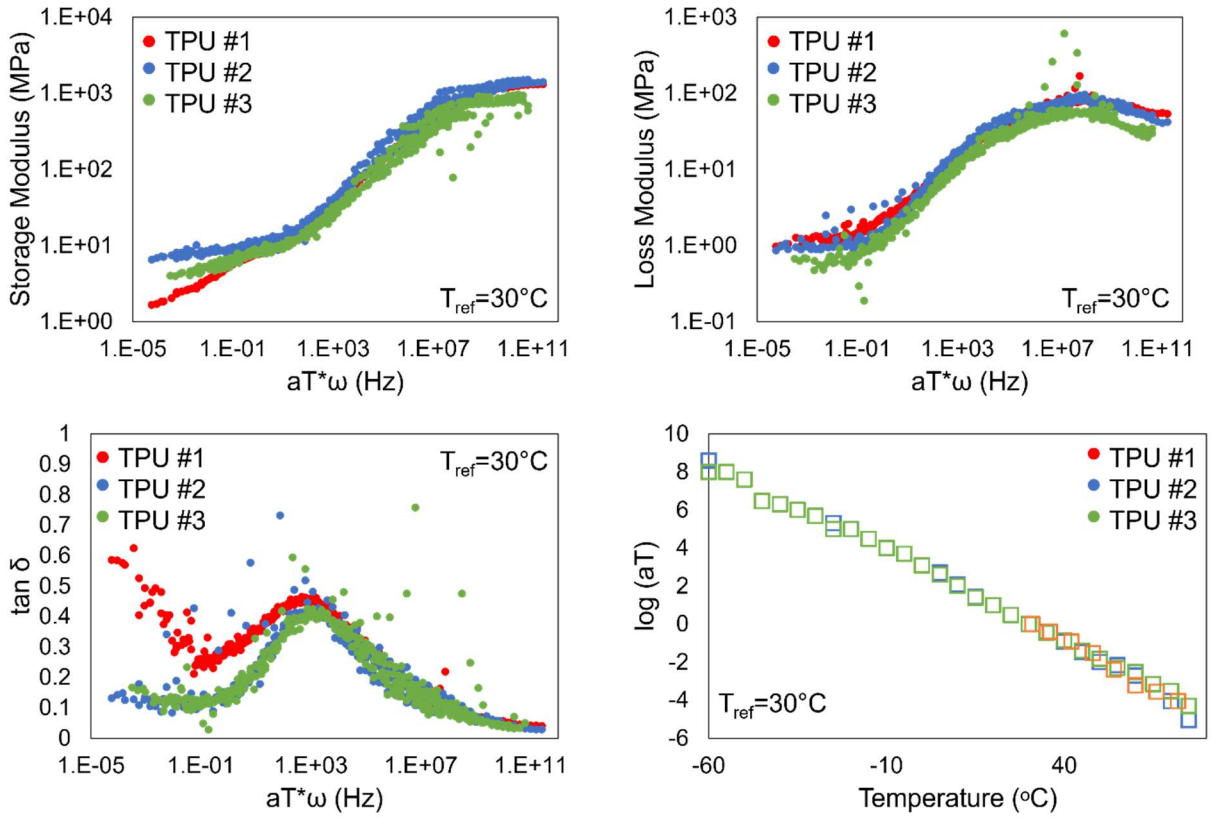

Fig. 45: Frequency sweeps for standard TPUs. Plots show the storage modulus (top left), loss modulus (top right), and tan δ (bottom left), as well as the shift factor plot (bottom right). The results are generally the same across all of the standard TPUs, although there is some obvious variation in the storage modulus and tan delta plots at small frequencies.

The DMA results are generally very similar for each of the standard TPUs. This is especially evident in the shift factor plots, which are nearly identical for each TPU. There is, however, some variation at lower frequencies in the storage modulus and tan δ plots. At these lower frequencies, there is a drastic decrease in the stiffness of TPU #1, which was the worst performing TPU for the wedge tests. TPU #2, the best performing interlayer for the wedge tests, on the other hand, maintains a higher stiffness at these smaller frequencies. Between ~15 Hz and ~5×10^{-5} Hz, the stiffness of TPU #2 decreases by ~85%, as opposed to TPU #1, which decreases by about only ~45% over the same range. This lower frequency range corresponds to higher temperatures, such as those studied in the wedge tests. The different stiffness values observed in the different TPUs could give a possible reason for their differing performances observed in the wedge tests and indicate a TPU stiffness below which the system becomes more prone to delamination.

3.2.3 Stiff TPU

While TPU #4 was classified as the stiff TPU since it had the highest secant modulus at room temperature, the time and temperature dependence on viscoelastic materials described in section 1.5 must still be considered. Fig. 46 shows the frequency sweeps obtained for TPU #4 compared to the frequency sweeps for the standard TPUs. DMA tests on TPU #4 were conducted from 30°C to 75°C unlike the standard TPUs, which were tested from -60°C to 75°C. This results in a smaller frequency range for the master curve for TPU #4.

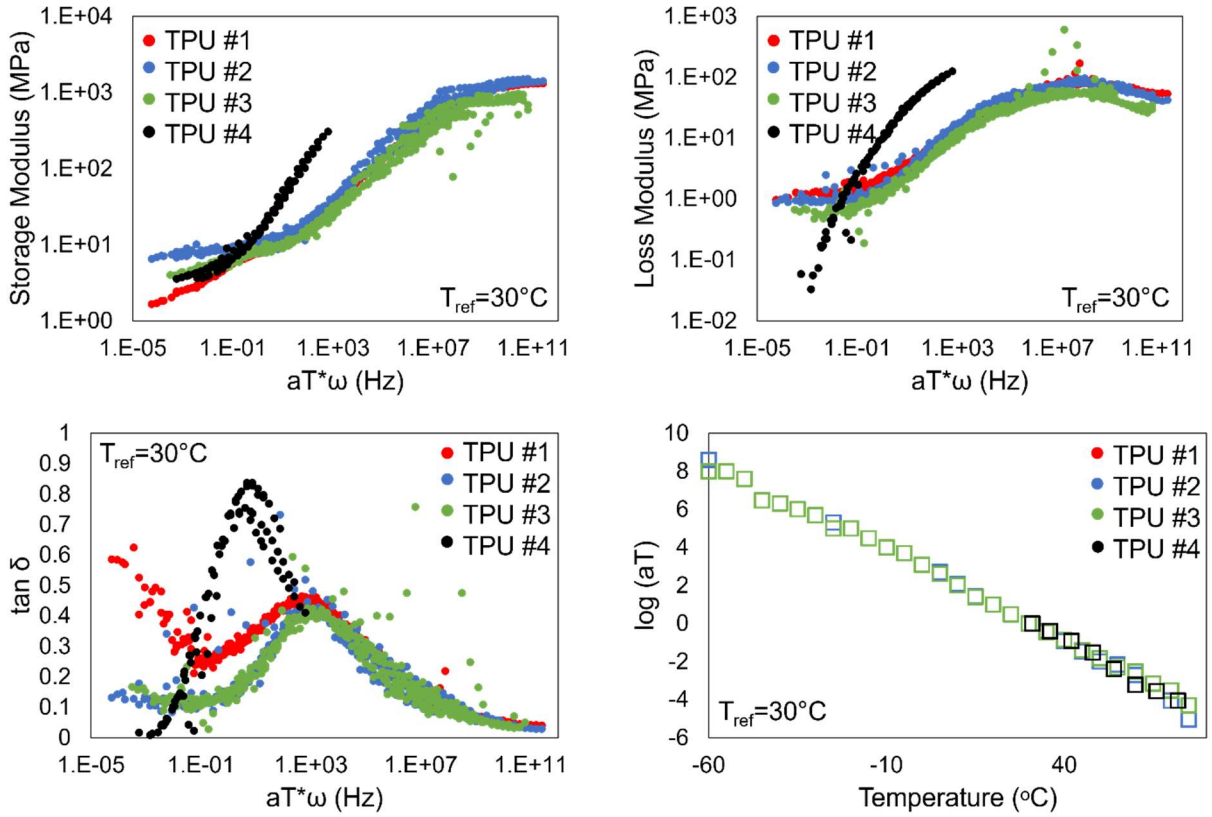

Fig. 46: Frequency sweeps for TPU #4 compared to the standard TPUs. Plots give the storage modulus (top left), loss modulus (top right), tan δ (bottom left), and the shift factor plot (bottom right) used to create the other plots. The results indicate that classifying TPU #4 as a stiff TPU is valid given its higher stiffness at higher frequencies.

The DMA results for TPU #4 confirm that it is indeed stiffer than the standard TPUs, not only at room temperature, but at lower temperatures and higher frequencies. The large difference in stiffness could give a possible reason for the drastic difference in the wedge test results obtained for standard TPU samples compared to those for TPU #4, as seen in section 3.1.4; however, literature has shown that stiffness of a material does not generally affect the formation of cavities. Kim showed in [73], however, that for silicone gels, while stiffer materials led to higher fracture energies and more spherical and sustaining cavities when stretched, there was no direct correlation between stiffness and cavitation persistence. It was instead suggested that the correlation is due to other material parameters including nonlinear elasticity or failure properties. These results were

also the basis for the Volkersen lengths discussed in section 3.1.4, where the values for the storage moduli at various temperatures were provided for TPU #4 in Table 3.

3.2.4 Other interlayers

As noted previously, polyvinyl butyral (PVB) has historically been the most commonly used interlayer for ballistic glass systems. In order to compare the viscoelastic nature of TPUs with PVBs, DMA testing was done for two different PVB interlayers. As in the tests on TPU #4, the tests for the PVBs were conducted from 30°C to 75°C, resulting in a smaller frequency range for the master curve for TPU #4. Fig. 47 shows the frequency sweeps obtained for the PVBs compared to the frequency sweeps for the TPUs.

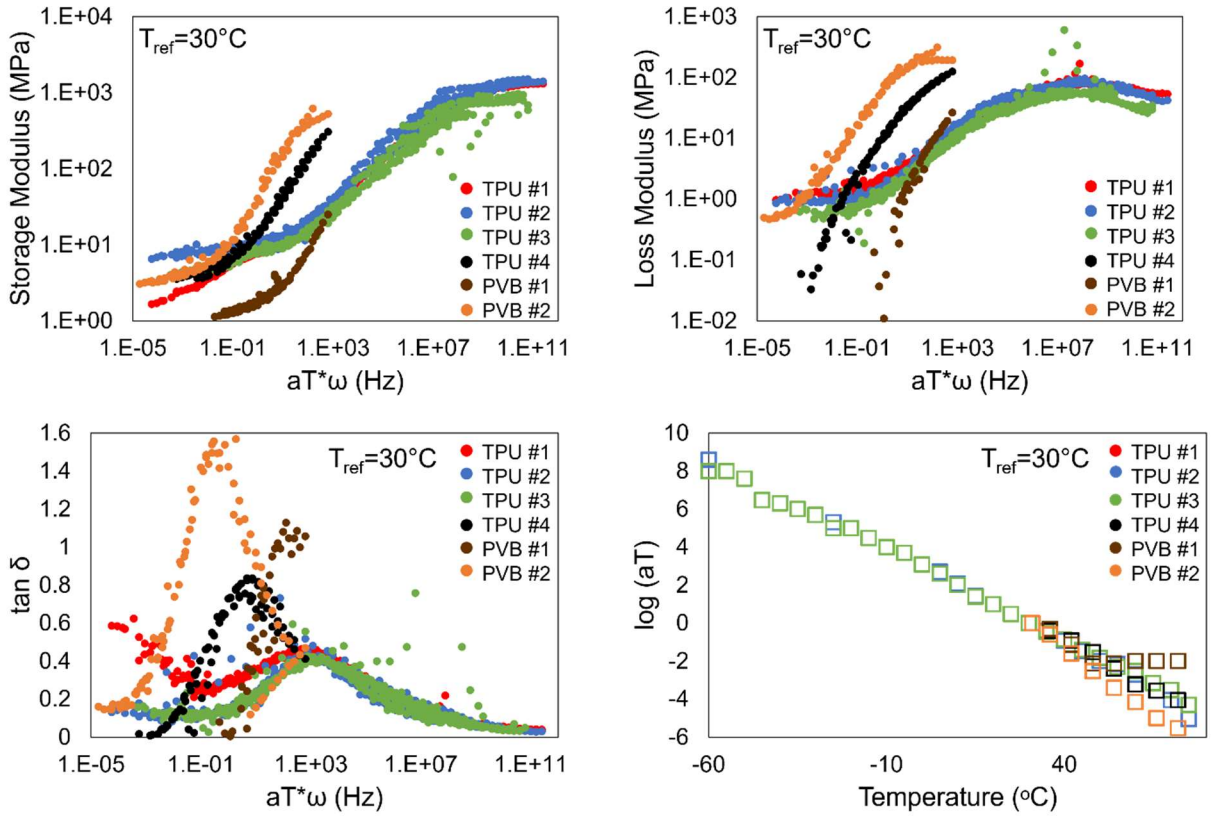

Fig. 47: Frequency sweeps for two PVB interlayers compared to the TPUs. Plots give the storage modulus (top left), loss modulus (top right), tan δ (bottom left), and the shift factor plot (bottom right) used to create the other plots.

PVB #1 behaves very differently from the TPUs with a much smaller stiffness than each of the interlayers tested. PVB #2, on the other hand, behaves more similarly to TPU #4, and at large frequencies has a very similar stiffness to both TPU #4 and TPU #3. These results could be used in future studies to explore the durability of laminated glass systems using PVB interlayers and in making determinations for the most durable interlayer. It might be assumed that PVB #2 is a more

durable material than PVB #1 since it maintains a higher stiffness at higher temperatures, similar to the better performance of TPU #3 compared to TPU #1.

4 Conclusions

This project involved a complex problem spanning a number of fields including fracture mechanics, materials science, and polymer science. Several conclusions can be drawn from this study.

1. **The durability of different TPU-polycarbonate systems can be compared using the wedge test method.** In this thesis, three standard TPUs were evaluated. Fig. 25 indicated that TPU #2 provided the greatest resistance to delamination based on the crack growth over time, and TPU #1 provided the least resistance. Although requiring more time for testing than the other methods cited in section 1.2, the wedge tests were a simple and effective method for comparing the durability of different systems and allowed for multiple replicates to be tested at various conditions simultaneously. Apart from the few outliers mentioned, these results were consistent across multiple replicates of wedge specimens at different humidity and temperature conditions. While the wedge specimen geometry is different than most service applications for laminated glass systems, the wedge test is still a potentially useful method for comparing the durability of different TPUs. Experiments conducted by JNI on systems with different geometries agreed with the results from the wedge tests showing TPU #2 to be the best interlayer and TPU #1 to be the worst.

2. **The adhesive thickness of a wedge specimen has a significant effect on the estimation of its energy release rate using simple beam theory**. For a wedge test, the displacement of the specimen is fixed by the inserted wedge. The SBT method assumes that the two adherends of a wedge specimen are essentially cantilever beams, and the deflection of each beam is half the thickness of the wedge. The two adherends are initially separated by an adhesive, giving the wedge specimen an effective opening displacement. For systems with a thin adhesive on the level of micrometers, like those used by Cognard in [30], the effect is so small as to be negligible, and the opening displacement between the adherends is therefore ignored. For thicker adhesives, however, like those used in this thesis with a thickness on the level of millimeters, the effect cannot be ignored. Fig. 14 indicated that accounting for the thickness of the adhesive, for the specimens used in this study, can reduce the calculated energy release rate significantly, by almost an order of magnitude.

3. **The compliance of the adhesive used in a wedge test has a significant effect on the estimation of its energy release rate.** For methods like SBT, the compliance of the adhesive is ignored, meaning that displacement and rotation are assumed to be zero at the axial position corresponding to the debond tip for a wedge test specimen with a relatively thick and/or soft adhesive. The compliance, however, plays a significant role. A method to account for this compliance is Winkler's beam on elastic foundation method, which assumes that the restoring force of the adhesive is directly proportional to its displacement, thereby modeling the adhesive as a system of independent springs. A fourth order differential equation is used to define the displacement of the adhesive. From this

displacement, the compliance of the adhesive can be calculated and substituted into the expression for the energy release rate. Fig. 16 indicated that accounting for the compliance of the adhesive can have a significant effect on the energy release rate. Depending on the type of TPU, the adhesive compliance can reduce the calculated energy release rate by an order of magnitude or more at small crack lengths. This effect becomes smaller as the crack length increases. The reason for this is that the compliance of the debonded portion of the adherends begins to dominate as the debond length increases.

4. **The changing stiffness of a TPU interlayer in long time or high temperature conditions correlates to the crack growth experienced in a wedge test.** The dynamic mechanical analysis presented in Fig. 45 indicated that the storage modulus of each TPU was very similar except at instances of very low frequency (corresponding to high temperature or long times). Under high temperature conditions, the wedge tests using the TPU with the smallest storage modulus (TPU #1) were the worst performing and the most susceptible to changes in temperature, as shown in Fig. 25. In addition, the TPU with the highest storage modulus at very low frequencies (TPU #2) was the adhesive used in the best performing wedge tests. This confirms that there is an increase in durability for an adhesive joint whose interlayer remains stiffer at higher temperatures and longer times. Humidity conditions were also compared in the wedge tests and indicated different responses among the different TPUs, although dynamic mechanical analysis evaluation under varying humidity conditions has not been conducted.

5. **There is a correlation between sample preparation and the durability of wedge samples.** Wedge tests prepared with a plasma surface treatment were generally shown to decrease the crack growth of the wedge tests, as indicated by Fig. 44.

5 Future work

The wedge test proved to be a useful method for comparing the durability of polycarbonate laminates. Many specimens and materials were observed over the course of this project. Despite the relative simplicity of the wedge test, however, it presented several challenges for data collection that have led to areas in which future research might be conducted. These areas are highlighted below.

1. **Residual stress in wedge specimens.** Perhaps the greatest challenge in data collection for the wedge test was evaluating how residual stress affected the samples. This was an overarching issue in cases of cavitation in stiff TPU samples and in end debonding. Crude calculations were conducted to evaluate the residual stress due to the Volkersen effect on the wedge test specimens in section 3.1.4. Future research, however, is recommended to develop a better understanding of the residual stress in the wedge geometries of this study as well as in window applications and how these residual stresses are affected by environmental aging.

2. **Cavitation in wedge specimens.** Firstly, a distinction should be made between cavitation and debonding in a wedge specimen. At the early stages of this project, both cavitation and debond length were used to define a crack length that was then used to calculate the energy release rate. While some studies have attempted to calculate G from cavitation [74,

75], both simple beam theory and beam on elastic foundation assume that this crack growth is the result of complete interfacial debonding. It does not account for any energy dissipated from cavitation, which was observed in almost every wedge sample with TPU. Future studies should distinguish between these two fracture modes and address them separately when recording data. Furthermore, the source of the cavitation in wedge specimens remains largely unknown. Some samples resulted in cavitation at the crack tip at the very beginning of the tests. Other samples resulted in cavitation throughout the length of the specimen. Future work is encouraged to explore which systems are more prone to cavitation and the source – whether environmental or wedge-induced – for the cavitation.

3. **End effects in wedge specimens.** Secondly, careful attention should be given to end effects when measuring the crack length induced by a wedge in the wedge test. The energy release rate in this thesis was calculated considering the crack as it grew from the wedge end of the sample to the opposite end. As shown in Fig. 17, however, an additional crack began to grow from the opposite end of the beam toward the wedge end. In some data collection, this additional crack was measured as the new crack length, as measured from the wedge end of the sample. Future work is encouraged to explore the source of this end debonding and its effect on the BoEF model.

4. **Correlation between crack growth experienced in wedge test and the viscoelastic effect of a TPU interlayer from humidity conditions.** Thirdly, while this work involved the analysis of wedge samples exposed to varying temperature and humidity conditions, DMA was only conducted at varying temperatures. By conducting DMA at different humidity conditions, further explanations might be given for the durability of the different wedge test systems.

5. **Effect of potting materials and edge seals on the wedge test.** Finally, while wedge tests were conducted on both potting materials (in sections 3.1.6) and edge seals (in section 3.1.7), the results of these tests were largely inconclusive due to large variability among the samples. While the wedge test can still be used to show comparisons between the different potting materials and edge seals, careful attention should be given to consistency in sample preparation across each of the specimens. Future work on the comparison of systems with different potting materials and edge seals is encouraged.

In summary, wedge tests were conducted to simultaneously compare the delamination of wedge specimens under various temperature and humidity conditions, and methods for analyzing the fracture mechanics of these tests were compared. Dynamic mechanical analysis was utilized to compare the viscoelastic effects of the TPUs. Overall, these methods have been shown to be a reliable process for analyzing the durability of adhesive joints in laminated polycarbonate systems with a TPU interlayer.

References

[1] M. Martín, X. Centelles, A. Solé, C. Barreneche, A. I. Fernández, and L. F. Cabeza, "Polymeric interlayer materials for laminated glass: a review," *Construction and Building Materials,* vol. 230, 116897, 2020, doi: 10.1016/j.conbuildmat.2019.116897.

[2] J. C. Wood, "Improvements in Glass Screens, Windows, and the like for Motor Cars and other Vehicles," GB Patent 9972 Patent Appl. GB190509972DA·1905-05-11, 1905.

[3] G. F. Freeguard and D. Marshall, "Bullet-resistant glass: a review of product and process technology," *Composites,* vol. 11, no. 1, pp. 25-32, 1980, doi: 10.1016/0010-4361(80)90018-X.

[4] M. Teotia and R. K. Soni, "Polymer interlayers for glass lamination: a review," *International Journal of Science and Research,* vol. 3, no. 8, pp. 1264-1270, 2014, doi: 10.1016/j.conbuildmat.2019.116897.

[5] E. M. Pint, J. Fleming, G. Germanovich, and L. Muggy, *Addressing Ballistic Glass Delamination in the Marine Corps Tactical Vehicle Fleet*. Santa Monica, CA: Rand Corporation, 2018.

[6] M. Grujicic, W. C. Bell, and B. Pandurangan, "Design and material selection guidelines and strategies for transparent armor systems," *Materials and Design,* vol. 34, pp. 808-819, 2012, doi: 10.1016/j.matdes.2011.07.007.

[7] M. H. Merrill, "Assessment of adhesive bond strength for long-life performance," presented at the International Mechanical Engineering Conference and Exposition, Virtual, 2020.

[8] X. Centelles, M. Martin, A. Sole, J. R. Castro, and L. F. Cabeza, "Tensile test on interlayer materials for laminated glass under diverse ageing conditions and strain rates," *Construction and Building Materials,* vol. 243, p. 118230, 2020, doi: 10.1016/j.conbuildmat.2020.118230.

[9] A. Frick and A. Rochman, "Characterization of TPU-elastomers by thermal analysis (DSC)," *Polymer Testing,* vol. 23, pp. 413-417, 2004, doi: 10.1016/j.polymertesting.2003.09.013.

[10] N. MacAloney, A. Bujanda, R. Jensen, and N. Goulbourne, "Viscoelastic characterization of aliphatic polyurethane interlayers," Army Research Laboratory, Aberdeen Proving Ground, MD, 2007.

[11] T. Haná, M. Vokác, M. Eliásová, and K. V. Machalická, "Experimental investigation of temperature and loading rate effects on the initial shear stiffness of polymeric interlayers," *Engineering Structures,* vol. 223, p. 110728, 2020, doi: 10.1016/j.engstruct.2020.110728.

[12] K. Sakai and S. A. Nassar, "Polycarbonate-to-polycarbonate single lap joints with polyurethane film adhesive," presented at the Automotive Composites Conference and Exhibition, 2017.

[13] M. Eliášová, M. Vokáč, and K. Machalická, "Influence of polymeric interlayers on the stress distribution in laminated glass panes," in *22nd Annual Conference of Engineering Mechanics*, Svratka, Czech Republic, 2016.

[14] G. Rivers and D. Cronin, "Influence of moisture and thermal cycling on delamination flaws in transparent armor materials: thermolpastic polyurethane bonded glass-polycarbonate laminates," *Materials and Design,* vol. 182, p. 108026, 2019, doi: 10.1016/j.matdes.2019.108026.

[15] J. Gablin, J. Brar, and T. H. Miller, "Design specification for transparent armor for the mine resistant ambush protected (MRAP) family of vehicles," USMC PEO-Land Systems, Quantico, VA, 2013.

[16] K. Leighton, J. Carberry, W. Serafin, T. Avery, and D. Templeton, "Transparent armor for the new standard in transparent battle performance," Schott Diamond Armor LLC 2011.

[17] D. A. Dillard, "ESM 5264 Mechanics of Adhesive Bonding & Interaces: 10. Fracture Mechanics (Monolithic): An introduction to fracture mechanics," Virginia Polytechnic Institute and State University, Class Lecture, 2019.

[18] J. Brunet, B. Pierrat, and P. Badel, "Review of Current Advances in the Mechanical Description and Quantification of Aortic Dissection Mechanisms," *IEEE Reviews in Biomedical Engineering,* vol. 14, pp. 1-1, 01/03 2020, doi: 10.1109/RBME.2019.2950140.

[19] J. M. Gorman and M. D. Thouless, "The use of digital-image correlation to investigate the cohesive zone in a double-cantilever beam, with comparisons to numerical and analytical models," *Journal of the Mechanics and Physics of Solids,* vol. 123, pp. 315-331, 2019, doi: 10.1016/j.jmps.2018.08.013.

[20] J. W. Obreimoff, "The splitting strength of mica," in *Proceedings of the Royal Society of London*, 1930, vol. 127, no. 805, pp. 290-297, doi: 10.1098/rspa.1930.0058.

[21] J. A. Marceau and J. C. McMillan, "Exploratory Development on Durability of Adhesive Bonded Joints," Boeing Commerical Airplane Company, Seattle, Washington, 1976.

[22] J. L. Cotter and R. Kohler, "The influence of surface pretreatment on the durability of adhesively-bonded aluminium alloys in humid and corrosive environments," *International Journal of Adhesion and Adhesives,* vol. 1, no. 1, pp. 23-28, 1980, doi: 10.1016/0143-7496(80)90030-5.

[23] A. J. Kinloch, L. S. Welch, and H. E. Bishop, "The locus of environmental crack growth in bonded aluminum alloy joint," *The Journal of Adhesion,* vol. 16, no. 3, pp. 165-177, 1984, doi: 10.1080/00218468408074915.

[24] W. Brockmann, O. D. Hennemann, H. Kollek, and C. Matz, "Adhesion in bonded aluminum joints for aircraft construction," *International Journal of Adhesion and Adhesives,* vol. 6, no. 3, pp. 115-143, 1986, doi: 10.1016/0143-7496(86)90016-3.

[25] K. B. Armstrong, "Long-term durability in water of aluminum alloy ahesive joints bonded with epoxy adhesives," *International Journal of Adhesion and Adhesives,* vol. 17, no. 2, pp. 89-105, 1997, doi: 10.1016/S0143-7496(96)00038-3.

[26] *Standard Test Method for Adhesive-Bonded Surface Durability of Aluminum (Wedge Test)*, ASTM D3762-98, ASTM-International, West Conshohocken, PA, USA, 2021.

[27] R. D. Adams, J. W. Cowap, G. Farquharson, G. M. Margary, and D. Vaughn, "The relative merits of the Boeing wedge test and the double cantilever beam test for assessing the durability of adhesively bonded joints, with particular reference to the use of fracture

mechanics," *International Journal of Adhesion and Adhesives,* vol. 29, no. 6, pp. 609-620, 2009, doi: 10.1016/j.ijadhadh.2009.02.010.

[28] J. P. Sargent, "Durability studies for aerospace applications using peel and wedge tests," *International Journal of Adhesion and Adhesives,* vol. 25, no. 3, pp. 247-256, 2005, doi: 10.1016/j.ijadhadh.2004.07.005.

[29] J. Cognard, "Use of the wedge test to estimate the lifetime of an adhesive joint in an aggressive environment," *International Journal of Adhesion and Adhesives,* vol. 6, no. 4, pp. 215-220, 1986, doi: 10.1016/0143-7496(86)90008-4.

[30] J. Cognard, "The Mechanics of the Wedge Test," *The Journal of Adhesion,* vol. 20, no. 1, pp. 1-13, 1986, doi: 10.1080/00218468608073236.

[31] L. Skec, G. Alfano, and G. Jelenic, "Enhanced simple beam theory for characterising mode-I fracture resistance via a double cantilever beam test," *Composites Part B,* vol. 167, pp. 250-262, 2019, doi: 10.1016/j.compositesb.2018.11.099.

[32] O. A. Bauchau and J. I. Craig, "Euler-Bernoulli beam theory," in *Structural Analysis*, O. A. Bauchau and J. I. Craig Eds. Dordrecht, Netherlands: Springer, 2009, pp. 173-221.

[33] D. R. Arnott and M. R. Kindermann, "Constant displacement rate method for testing epoxy adhesive bonds," *The Journal of Adhesion,* vol. 48, no. 1-4, pp. 85-100, 1995, doi: 10.1080/00218469508028156.

[34] A. A. Griffith, "The phenomena of rupture and flow in solids," *Philosophical Transactions of the Royal Society of London,* vol. 221, pp. 163-198, 1921, doi: 10.1098/rsta.1921.0006.

[35] N. E. Dowling, *Mechanical Behavior of Materials*, 3rd ed. Upper Saddle River, NJ: Pearson Prentice Hall, 2007.

[36] J. G. Williams, "On the calculation of energy release rate for cracked laminates," *International Journal of Fracture* vol. 36, pp. 101-119, 1988, doi: 10.1007/BF00017790.

[37] B. D. Davidson, S. J. Gharibian, and L. Yu, "Evaluation of energy release rate-based approaches for predicting delamination grwoth in laminated composites," *International Journal of Fracture,* vol. 105, pp. 343-365, 2000, doi: 10.1023/A:1007647226760.

[38] D. A. Mendels and R. M. Shaw, "Determination of mode I energy release rate in composite laminates by the wedge test," *NPL Report,* MATC(MN)36, 2002.

[39] M. F. Kanninen and C.H.Popelar, "Advanced Fracture Mechanics." New York: Oxford University Press, 1985, pp. 158-161.

[40] D. A. Dillard, "ESM 5264 Mechanics of Adheisve Bonding & Interfaces: 13. Conducting Fracture Tests: Conducting fracture tests of bonded beams, bars, & blisters," Virginia Polytechnic Institute and State University, Class Lecture, 2019.

[41] K. Selby and L. E. Miller, "Fractue toughness and mechanical behaviour of an epoxy resin," *Journal of Materials Science,* vol. 10, pp. 12-24, 1975, doi: 10.1007/BF00541027.

[42] G. R. Irwin, "Fracture," in *Elasticity and Plasticity*. Berlin, Germany: Springer, 1958, pp. 551-590.

[43] K. P. Menard, *Dynamic Mechanical Analysis: A Practical Introduction*. Boca Raton, Florida, USA: CRC Press LLC, 1999.

[44] J. D. Menczel and R. B. Prime, "Thermal Analysis of Polymers: Fundamentals and Applications." Hoboken, New Jersey, USA: John Wiley & Sons, Inc., 2009, pp. 387-488.

[45] M. J. Bortner, "ESM 5264 Mechanics of Adhesive Bonding & Interaces: Intro to Polymer Rheology in Adhesive Applications," Virginia Polytechnic Institute and State University, Class Lecture, 2021.

[46] M. L. Williams, R. F. Landel, and J. D. Ferry, "The temperature dependence of relaxation mechanisms in amorphous polymers and other glass-froming liquids," *J. Amer. Chem. Soc.,* vol. 77, pp. 3701-3707, 1955, doi: 10.1021%2Fja01619a008.

[47] T. A. Instruments, "Understanding Rheology of Thermoplastic Polymers," in *Application Note TA 144*. New Castle, DE, USA: T.A. Instruments, pp. 1-8.

[48] *Standard Test Methods for Vulcanized Rubber and Thermoplastic Elastomers - Tension*, ASTM D412-16, ASTM-International, West Conshohocken, PA, USA, 2021.

[49] I. Baylakoglu, C. Hillman, and M. Pecht, "Characterization of some commercial thermally-cured potting materials," presented at the International IEEE Conference on the Business of Electronic Product Reliability and Liability, Hong Kong, 2003.

[50] M. Kempe, J. Wohlgemuth, D. Miller, L. Postak, D. Booth, and N. Phillips, "Investigation of a wedge adhesion test for edge seals," *Proceedings of SPIE,* vol. 9938, 993803-1, 2016, doi: 10.1117/12.2239161.

[51] D. Jungkuist and M. Moncur, "Environmental Seal Technology for Spaced Transparent Armor," US Patent 2011/0072961 A1 Patent Appl. 12/275,142, 2011.

[52] S. L. Kaplan and P. W. Rose, "Plasma surface treatment of plastics to enhance adhesion," *International Journal of Adhesion and Adhesives,* vol. 11, pp. 109-113, 1991, doi: 10.1016/0143-7496(91)90035-G.

[53] P. Atkins and J. Paula, *Physical Chemistry*, 10th ed. Oxford University Press, 2014.

[54] X. Li, J. Lu, J. Luo, H. Zheng, and G. Shao, "Effects of Cold Plasma Treatement on the Performance of Polyurethane Laminated Glass," *Plasma Chemistry and Plasma Process,* vol. 34, pp. 207-215, 2014, doi: 10.1007/s11090-013-9494-0.

[55] R. C. Hibbeler, *Mechanics of Materials*, 8th ed. Upper Saddle River, NJ: Pearson Prentice Hall, 2011.

[56] E. Winkler, *Die Lehre von der Elasticitaet und Festigkeit mit besondere Rueckshicht auf ihre Anwendung in der Technik, fuer polytechnische Schulen, Bauakademien, Ingenieure, Maschienenbauer, Architecten, etc.* Prague: Dominicus, 1867.

[57] D. A. Dillard, B. Mukherjee, P. Karnal, R. C. Batra, and J. Frechette, "A review of Winkler's foundation and its profound influence on adhesion and soft matter applications," *Soft Matter,* vol. 14, p. 3669, 2018, doi: 10.1039/c7sm02062g.

[58] D. A. Dillard, "Bending of plates on thin elastomeric foundations," *Journal of Applied Mechanics,* vol. 56, pp. 382-386, 1989, doi: 10.1115/1.3176093.

[59] R. H. Plaut and D. A. Dillard, "Peeling of finite-length plates from an elastomeric foundation: a 1D Cylindrical Bending Solution," *Journal of Applied Mechanics,* vol. 90, pp. 091001-1, 2023, doi: 10.1115/1.4062493.

[60] R. H. Plaut, D. Hwang, C. Lee, M. D. Bartlett, and D. A. Dillard, "Peeling of finite-length elastic on Winkler foundation until complete detachment," *International Journal of Solids and Structures,* vol. 256, p. 111944, 2022, doi: 10.1016/j.ijsolstr.2022.111944.

[61] S. W. Case, "Finite element analysis of wedge tests on adhesively-bonded elastic beams with finite compliance adhesives," Virginia Polytechnic Insitute and State University, 2023.

[62] B. Mukherjee, R. C. Batra, and D. A. Dillard, "Edge debonding in peeling of a thin flexible plate from an elastomer layer: a cohesive zone model analysis," *Journal of Applied Mechanics,* vol. 84, no. 2, 2017, doi: 10.1115/1.4034988.

[63] B. Mukherjee, R. C. Batra, and D. A. Dillard, "Effect of confinement and interfacial adhesion on peeling of a flexible plate from an elastomeric layer," *International Journal of Solids and Structures,* vol. 110-111, pp. 385-403, 2017, doi: 10.1016/j.ijsolstr.2016.09.004.

[64] B. Mukherjee, D. A. Dillard, and R. C. Batra, "On preferential debonding during demolding of a sandwiched elastomeric layer," *International Journal of Solids and Structures,* vol. 170, pp. 123-141, 2019, doi: 10.1016/j.ijsolstr.2019.04.018.

[65] B. Mukherjee, D. A. Dillard, R. B. Moore, and R. C. Batra, "Debonding of confined elastomeric layer using cohesive zone model," *International Journal of Adhesion and Adhesives,* vol. 66, pp. 114-127, 2016, doi: 10.1016/j.ijadhadh.2015.12.006.

[66] *Standard Test Method for Measurements of Fatigue Crack Growth Rates*, ASTM E647, ASTM-International, West Conshohocken, PA, USA, 2023.

[67] H. K. Mueller and W.G.Knauss, "The fracture energy and some mechanical properties of a polyurethane elastomer," *Journal of Rheology,* vol. 15, no. 2, pp. 217-233, 1971, doi: 10.1122/1.549209.

[68] C. Creton and M. Ciccotti, "Fracture and adhesion of soft materials: a review," *Reports on Progress in Physics,* vol. 79, 046601, 2016, doi: 10.1088/0034-4885/79/4/046601.

[69] C. W. Barney *et al.*, "Cavitation in soft matter," *PNAS,* vol. 117, no. 17, pp. 9157-9165, 2020, doi: 10.1073/pnas.1920168117.

[70] D. A. Dillard, "ESM 5264 Mechanics of Adhesive Bonding & Interfaces: 5. Shear Lag & Beam on Elastic Foundation: Classic Stress Transfer Concepts Relevant to Adhesive Bonds," Virginia Polytechnic Institute and State University, Class Lecture, 2019.

[71] O. Volkersen, "Die Nietkraftverteilung in zugbeanspruchten Nietverbindungen mit konstanten Laschenquerschnitten," *Luftfahrtfor schung,* vol. 15, pp. 41-47, 1938.

[72] *Standard Test Method for Tensile Properties of Plastics*, ASTM D638-14, ASTM-International, West Conshohocken, PA, USA, 2022.

[73] J. Y. Kim *et al.*, "Extreme cavity expansion in soft solids: Damage without fracture," *Science Advances,* vol. 6, no. 2375-2548, 2020, doi: 10.1126/sciadv.aaz0418.

[74] J. Kang, C. Wang, and S. Cai, "Cavitation to fracture transition in a soft solid," *Soft Matter,* vol. 13, pp. 6372-6376, 2017, doi: 10.1039/c7sm01479a.

[75] M. L. Williams and R. A. Schapery, "Spherical flaw instability in hydrostatic tension," *International Journal of Fracture Mechanics,* vol. 1, pp. 64-72, 1965, doi: 10.1007/BF00184154.